Velocity and Attenuation Analysis of Gulf Coast Sediments using Vertical Seismic Profiling

by

James Raymond Wingo

B.S., Massachusetts Institute of Technology
(1980)

SUBMITTED TO THE DEPARTMENT OF
EARTH AND PLANETARY SCIENCE
IN PARTIAL FULFILLMENT OF THE
REQUIREMENTS FOR THE
DEGREE OF

MASTER OF SCIENCE IN

EARTH AND PLANETARY SCIENCE

at the

MASSACHUSETTS INSTITUTE OF TECHNOLOGY

JUNE,1981

Signature of Author _____
Department of Earth and Planetary Science
May 22,1981

Certified by _____
Nafi M. Toksoz
Thesis Supervisor

Accepted by _____
Chairman, Departmental Graduate Committee

Velocity and Attenuation Analysis of Gulf Coast Sediments using Vertical Seismic Profiling

by

James Raymond Wingo

Submitted to the Department of Earth and Planetary Science on May 22, 1981 in partial fulfillment of the requirements for the degree of Master of Science in

Geophysics

ABSTRACT

The elastic and anelastic properties of shallow sediments are becoming increasingly important for detailed understanding of earth properties. In order to study the velocity and attenuation properties of shallow sediments near the Gulf Coast, a vertical seismic profile was completed for a 1650 ft. deep gas well. Signals from an impulsive seismic source were received by a three-component geophone clamped down the well. Arrivals were recorded in 10-ft. intervals, from well base to the surface.

Attenuation analysis techniques included alignment and then summation of traces from a series of depths to yield average properties over comparison intervals. Attenuation computations were completed using a spectral ratio method. For compressional waves, minimum interval size was a depth range approximately equal to the wavelength of the dominant frequency component of comparison waveforms. P-wave attenuation increased markedly through the gas zone. The average Qp dropped from about 35 to 5. The frequency content of the source compressional waveform changed over time, so monitor geophone calibrations were used.

Shear wave attenuation was relatively constant; average Q_S was about 20. Minimum s-wave attenuation computation interval size was larger than that for p-waves, because of source consistency problems.

Velocities were a function of depth more than rock type. Average velocities for the three rock types encountered ranged over only only 1%. Shear velocities increased more strongly with depth, as the ratio V_p/V_S decreased from about 6.8 to 3.6 from the surface to well base.

Thesis Supervisor: Dr. M. N. Toksoz

Title: Professor of Geophysics

Contents

Introduction

The seismic properties of shallow sediments are complex and highly variable, yet are increasingly important for detailed examination of earth structure.

For example, in exploration seismology it is important to learn more about local variations in shallow shear wave velocities and their relationship to p-wave velocities, in order to prepare common-depth-point stacks of s-wave data. In earthquake engineering, the susceptibility of structures to earthquake damage depends on the properties of near-surface sediments. In order to study shallow sediment properties, we analyzed compressional and shear wave data acquired through use of a vertical seismec profiling (VSP) technique.

Combined study of both p-and s-wave properties is superior to p-wave analysis alone for delineation of rock types and pore fluid saturation condition, because p-and s-wave characteristics are differentially affected by changes in medium properties. Toksoz et al (1976) discussed the effects of changes in rock type and pore fluid on rock velocities and attenuation of seismic waves (Toksoz et al,1979). Tatham and Stoffa (1976), and Gardner and Gregory (1974) discussed the value of applying both p-and s-wave data waves to problems in exploration seismology.

Previous work on shallow in-situ s-and p-wave relationships has been done by Tullos and Reid (1958), and Gardner and Harris (1968), both for Gulf coast sediments. Benzing (1976) present-

ed results of laboratory studies of p-and s-waves in carbonates and sandstones, finding higher velocities and V_p/V_s ratios for sands than carbonates.

Considerable work has been done in Japan on p-and s-wave propagation properties (mainly for earthquake engineering purposes). Ohta et al (1980) used VSP in a study near Tokyo, generating velocity structures for p-and s-waves to a depth of about 3 km. A review of research on dynamic properties of sediments is given in a paper by Imai et al (1979).

In addition to being intended to gain information about near-surface p-and s-wave velocities, this experiment was designed to determine whether there is a detectible change in the rate of attenuation and velocity of seismic waves as they propagate through a gas zone. This involved the problem of finding resolution limits for the technique of vertical seismic profiling under normal field conditions.

VSP is a technique for seismic data acquisition which is characterized by the detection down a well of waveforms generated by a source at the surface. Conventional surface geophone array positioning has the disadvantage that signals must travel to the receivers through the highly attenuation and relatively low-velocity weathered layer just below the surface. Wuenschal (1974) noted that much of the source-generated seismic noise is caused by multiple scattered and converted waves radiating from near-surface inhomogeneities. He found that recording of signals by geophones well below the surface can improve the signal to noise

ratio markedly.

Because of the superior data resolution it provides, VSP has been utilized in analysis of medium properties over seismic frequencies. Dix (1945) discussed simple velocity determination techniques for down-well tests. Tullos and Reid (1958) completed a velocity and attenuation study for a shallow Gulf Coast well, obtaining values of the attenuation constant for layered sediments despite significant reflection interference.

More recently, Lash (1980) presented results of a p-and s-wave VSP study focusing on converted wave generation. Stewart et al (1981) found increased attenuation and reduced velocity for before-and after analysis of p-waves passing through a fracture zone.

A comprehensive treatment of VSP, with discussion of techniques and results, is by Gal'perin (1974).

The potential for VSP applications was further explored by Wyatt (1981), who utilized synthetic methods to generate a VSP section which displayed waveform transmission properties in both time and depth. Hardage (1981) compared synthetic seismograms created from VSP data to that generalized from sonic log data and found that in one instance VSP data, despite heavy tube wave contamination, gave superior agreement with surface reflection data.

This study yielded p-and s-wave velocity and attenuation structures for shallow Gulf Coast sediments. Compressional wave velocity and attenuation were notably affected upon passing through a gas zone, while shear wave properties were

less strongly altered. For attenuation analysis, traces from consecutive depth points were aligned for the event of interest and then were summed to yield average interval properties. Maximum resolution for was at least equal to the dominant wavelength for each wave type, due to effects of interference and source variation.

Velocity structures were generated through use of a two-dimensional straight-raypath ray tracing program, and were found to correlate well with sonic-log data. Resolution depended on wavelength and interval velocity, and shear wave information was better constrained over depth.

Geology

Sediments in the region and at depths for which the survey took place were of Quaternary age. The shallowest marker layer was at 2100 ft., below the deepest survey depth.

The well penetrated two shallow gas zones which were surrounded by layers of poorly consolidated sediments. For velocity analysis four classifications of sediments, determined from well log analysis, were used to distinguish facies. They were: near-surface sediments, sands, siltstone, and clayey shales. In percentages, the strata were roughly 65% shales, 20% sands, and 15% silts. Sands were dominant near the surface, while shale was most common near the well bottom.

The strata were very unconsolidated. Core samples taken below 1,000 feet added little lithologic information. Washout was a recurrent problem, compromising well log information and causing vibration of the horizontal components of the downhole geophone at several locations.

The strata were thin. In the velocity analysis, thirty-one layers with an average thickness of 50 feet were used. Boundaries were often defined across gradual changes in sediment content. There was only one good reflector, causing a "bright spot" at 1,320 feet. Overall, the lithology is best described as a series of thin beds with continuously varying proportions of sand, mud, and silt.

Figures 3-4 are plots of strata types down the well.

Experimental Overview and Geometry

Testing was carried out for three sources fixed in surface positions, with a geophone moving up through depth intervals consistent for each source. The next section, on survey procedure, describes the experimental process in greater detail.

The survey utilized three sources, a sliding weight drop machine called the thumper, a vacuum gun, and a shear wave vibroseis truck. The thumper was the only source used for the velocity and attenuation analysis in this paper, because of the superior spatial resolution it provided. (Appendix 1 describes t the source and the recording apparatus.)

The three sources generated pulses from positions south of the well, at an average distance of about 250 feet (see figure 2). The vacuum gun and thumper were at a separation of about fifty feet, with the thumper 270 feet from the well at an azimuth of S25^0 57"W, and the vacuum gun northwest of the thumper, S36^0 12"W relative to and 260 feet away from the well. The vibrator was 244 feet from the well at an angle of S40^0 57"E, and 283 feet northwest of the thumper.

A three-component monitor geophone was buried halfway between the thumper and well, about ten feet off the line between thumper and well. It was at a depth of about twenty-five feet.

The well itself was cased and cemented , and extending to a depth of 1650 feet.

Source geometry was partly dictated by fiel conditions.

Obstacles included the presence of a large mudpit between thumper and well, woods, and uniformly muddy terrain. The sources were kept stationary throughout the survey, and dry cement was used to preserve and improve the coupling between the thumper and ground.

Procedure

Field procedure was to complete thumper shots for 10-ft. downhole geophone spacings, and vacuum gun and vibroseis measurements every 100 feet.

For each depth, the thumper generated four pulses, two for each of two weight ramp orientations symmetric about a line from the thumper to the well. In each instance the ramp was positioned at an angle of 45° to the horizontal. The two positionings will here be referred to as "east" and "west," according to the weight ramp position relative to the line to the well.

The thumper orientations were so chosen in order to generate both compressional and shear waves; to minimize generation of SV-waves, and to produce SH first arrivals of opposite polarities (for travel-time and shear attenuation calculations). Figure 5 is an example of the relative amplitudes of shear and compressional waves produced by the thumper as recorded by the downhole geophone at 1,500 feet.

After the thumper had completed pulse generations for for the first clamping of the downhole geophone at 1,650 feet, the downhole phone was moved up to 1,640 feet, and so on until it reached 1,330 feet. The thumper retained the same polarity for the first pulse at a new geophone depth as for the last pulse at the preceding depth. In addition, every time the weight chassis moved to a new orientation, the operator fired a few test shots until he was satisfied

that the couple between source and ground was adequate.

After the thumper reached 1,330 feet, it operated in alternation with the vacuum gun for successive geophone movements of 100 feet until the geophone reached the surface. During this sequence, one source would complete all of its rounds, followed by the other, and at the next depth the order of shooting would reverse.

The geophone was lowered again to 1,320 feet after the final vacuum gun run at 30 feet, and for the remainder of the experiment the thumper was the only source used. Ten-foot geophone movements were standard except to avoid depths where gravity-weight arrivals had already been recorded during the vacuum gun sequence.

Recording instrument gains for thedownhole geophone were changed several times near the surface, but only once for shots below 600 feet (the shallow cutoff for attenuation analysis in this study): they were reduced 12 db for all three channels when the downhole geophone reached 620 feet.

Monitor geophone gains were changed once during the survey, just after all vacuum gun tests were completed.

The combined effects of 330 shots per orientation (excluding tests) and muddy field conditions created need for steps to improve the source-ground coupling frequently. Dry cement was therefore placed beneath the thumper ground pool when necessary. After each addition of cement, the thumper operator initiated several test shots to prepare the couple.

The survey lasted three days, but about half of that time was spent resolving logistical difficulties; the shooting itself ran continuously for about 36 hours.

Velocity Analysis

Compressional Waves Travel Times

Arrival time picks from the thumper source data were the inputs for compressional and shear wave velocity analysis. Plots with a time scale of 50 ms/inch were used for initial p-wave picks, and 20 ms/inch plots were later used for checking. This approach gave arrival times within a range of about $\pm$ 1.5 ms.

However, the usual human error involved in first-break measurement was accompanied by uncertainties engendered by recording instrument zero time variations. The recording instruments often cut in before or after the source began to generate its signal; the worst case was an apparent travel time difference of fifteen ms. between two first arrivals for different thumps traveling to the same depth point. Usually the range of variation in travel times to the same point was $\pm$2 ms.

This problem was resolved to within human picking error by examination of the monitor geophone arrival times. An average arrival time of 23 ms. from source to monitor phone was used to determine zero time differences, and lags thus computed varied in a manner consistent with the variations in travel time to the downhole geophone. The close downhole geophone spacings and the small and monotonic p-wave moveout of 2 or 3 ms. per spacing (except for those near-surface readings where head waves arrived first) helped to minimize

error. The net result is confidence in travel time picks still to within about 2 ms.

Figures 6-9 show the pattern of compressional waveform arrivals down the well.

Shear Waves Travel Times

Shear wave arrival times were less well fixed. There were the usual difficulties, including human error and zero time, as for p-waves.

But since accurate shear wave picks require overlays of rotated arrivals of opposite polarities, (see figure 10), the zero-time uncertainties were doubled. There were also difficulties in identification of shear arrivals because of low level noise due to tube wave and late-arriving compressional wave interference. Finally, the thumper source did not generate identical but reversed waveforms upon reorientation; this problem increased with time and differential compaction, and therefore was largest when the downhole geophone was shallowest.

The zero-time problem was corrected using p-wave monitor correction parameters, and arrivals were measured from overlay plots scaled to 40 ms/inch. Reversals were very weak near the surface, perhaps due to effects of tube wave arrivals and because of surface wave masking. There were also roughly 20 ringy, clipped, or dead depth points on the horizontal components of the downhole geophone. (There was

only one bad depth point for the vertical component. Poor cementing allowed much more horizontal than vertical geophone oscillation.) The shear wave arrival times are interpolated values in some cases. Nevertheless, consistent moveout patterns recorded over small spacings again helped greatly to increase shear wave arrival time measurement accuracy. Error ranges are $\pm$3 ms. at depth and $\pm$4 ms. near the surface. But spatially the shear wave error ranges are smaller than for compressional waves; the average Vp/Vs ratio is 4, while the errors range over roughly a factor of two. (This means that the shear wave velocity structure was better constrained in terms of layer depths and thicknesses.

Figures 11-16 are plots of shear wave arrival waveforms for the indicated geophone locations down the well, and figure 17 shows incidence times for shear and compressional waves as a function of depth.

Ray Tracing

After arrival time picking was completed, the real travel times were input to a flat-layer ray tracing program as standards for comparison with computed travel times. Two velocity structures were calculated by ray-tracing methods: one whose layer boundaries correlated with real lithologic boundaries, and one which was generated independent of lithology, with interfaces marked every 50 ft.

The software propagated rays to the well for a range

and density of initial incident angles specified by the user. It then interpolated to yield travel times at 10-ft. intervals (for which real travel times were also available). Another program compared computed travel times with real travel times, and it generated files with residuals for 10-and 100-foot intervals. The investigator used trial and error methods to minimize travel time differences. Appendix 2 contains a listing of the ray-tracing program.

For the lithologically-based velocity structure, layer boundary inputs to the modeling program were based on analysis of well log resistivity, SP, induction, sonic and density charts. A thirty-one layer model, with four general sediment classes (including the near-surface region as one class) was then used for ray-tracing analysis. However, although the average layer thickness is 50 feet, only eleven of the layers had thicknesses of over 90 feet, and thirteen were of thicknesses of ten to twenty feet. Velocities for the latter layers were determined beyond the modelling program's limits of resolution for the travel time picking constraints, and encountered uniqueness problems resolved by examination of information from the well logs. Their initial velocities were based on sonic log analysis, and were varied in a consistent manner for depth and lithology. Figure 18 is a plot of final computed velocities for the litholic model.

Comparison of the lithologic and fixed-block models shows that the two are very similar, with differences

primarily due to smoothing where lithologic layers are thin. For instance, in the 1300-1400 ft. region, where the average layer thickness for the lithologic model was less than 20 ft., the blocked model, like the lithologic model shows a lower velocity for the block including the gas region, but yields a smoothed average velocity for the deeper zone, contrasting with the lithologic model's (and sonic log's) greater acoustic differences. The higher resolution from the lithologic model in the second zone is beyond the resolution of ray-tracing modelling for the error constraints in this study.

The proceeding discussion summarizes velocity trends with rock type based on lithologic model analysis. Average velocities were based on layer velocities weighted according to layer thickness, so that the thickest layers, for which there is greatest certainty in interval velocity, are weighted most heavily.

Compressional Wave Velocities

Table 1 shows average velocities computed for the various sediment types. The table shows that velocities for the three classes are almost equal, with sand velocities averaging 6090 ft/s, silt speeds about 6075 ft/s, and shale velocities only slightly lower, at 6050 ft/s; the overall spread in velocities was only 1%. However, over 80% of the sands and almost all of the silts are in the shallower half of the well, where all velocities are lower. For the

shallower half of the well, where velocity changes due to rock type can be partly isolated from compaction effects, sand and silt velocities were equal to their whole-survey averages of 6090 and 6075 ft/s, respectively, while shale velocities were significantly lower, at 6010 ft/s. For all classes, the average top-half velocity was 5930 ft/s, the bottom-half average was 6210 ft/s, and the overall Vp was 6070 ft/s.

Shear Wave Velocities

Variation between shear wave velocities was a function of depth more than of strata type. For shales, the overall V_S was 1710 ft/s, with a top half average of 1600 ft/sec and a lower-half mean of 1770 ft/s.

Silts averaged 1450 ft/s through the survey depths, while sands were near 1300 ft/s.

Shear wave velocities increased strongly with depth. The top-half average speed was 1320 ft/s, the bottom-half average was 1750 ft/s, and the overall average was 1540 ft/s.

Vp/Vs Relationships

Vp/V_S values were most strongly indicative of the relatively rapid shear wave velocity increase with depth and compaction. (See figure 19.)

Shales, most prevalent at depth, had an overall Vp/V_S of 3.6. Sands, the dominant shallow sediment, had a Vp/V_S

of 4.6, while for silts the value was 4.2.

For the top half of the well, the average Vp/V_S was 4.5, and for the bottom portion it was 4.0; from top to base the mean was 4.2.

Sonic Log Comparisons

The velocity structure generated for compressional waves through ray-tracing methods was later compared to a velocity structure derived from sonic log travel times. Correspondence was close. Velocities from the sonic log were generally slightly lower than for the layered model (see figure 18), particularly near the surface.

As a further test, the sonic log velocity picks were averaged over ten-foot intervals and were then input as a 165-layer case to the ray-tracing program. Travel times computed using sonic log velocities were consistently greater than real travel times, with the greatest transit differences at shallow depths. Below 1,000 feet the travel time differences were within picking error. If washout and porosity were abnormally large near the surface, as other sources indicate, then this trend in residuals is not surprising. Figure 20 shows residuals as a function of depth for the sonic model.

Even assuming that in situ velocities are well-known, a straight-ray program like that used for this study will compute from the true velocities smaller transit times than would arise in real field tests, because real raypaths are

somewhat curved. Velocities discussed here for the layered model in p were chosen so that computed times would generate slightly negative travel time residuals within the range of picking error. The positive residuals for the sonic log model, which were consistently greater than picking error at shallow depths, indicate that sonic log velocities were probably significantly lower than real velocities in shallow regions.

Attenuation

Attenuation is a comprehensive term describing the energy loss of a wave as it travels through a medium. It results from interactions including reflection and refraction, geometric spreading, scattering, and absorption of energy by the material through which the wave propagates. In addition, constructive and destructive interference can cause apparent variations in measured attenuation over a range of frequencies.

All of these attenuation agents except absorption are elastic properties, whereas absorption includes anelastic losses, of which frictional interactions are probably the dominant component (Johnston et al,1979).

Early field work on seismic wave attenuation was done by Born (1945),who found that the frequency content of arrivals through shallow earth decreases exponentially with time. This led Born to assume propagation of plane seismic waves with amplitudes of the form:

$$A(f)=G(f,z)(e^{-\alpha zt})e^{i(2\pi ft-kz)}$$

where G depends on geometry,including reflections and $(1/z^2)$ geometric spreading; α is the attenuation coefficient; $k=2\pi/\lambda=2\pi f/V$; and V is phase velocity.

The attenuation coefficient usually increases linearly with frequency over a wide range of frequencies, including

the seismic range:

$$\alpha = \nu f$$

and ν is a constant which is characteristic of a given rock type, and which varies with saturation and pressure (Toksoz et al, 1979).

The value of ν for a particular rock sample can be determined by comparing the frequency spectrum of the sample with that of a known reference. The ratio of the natural logarithms of the respective amplitudes is:

$$\ln(A_1/A_2) = (\nu_2 - \nu_1) z f + \ln(G_1/G_2)$$

Assuming that G_1/G_2 does not depend on frequency, the slope of of the spectral ratio plot should be constant. If ν_1 is known or is very small, then the attenuation constant of the sample can be found directly (Toksoz et al,1979).

For VSP analysis, one can measure ν by assuming that waveforms propagate over the same, nearly vertical, raypaths until reaching the neighborhood of the shallower receiver. A comparison of spectra of the deeper and shallower receivers should be indicative of the attenuation through strata between the two measuring points. This assumption of similar raypaths improves with depth for VSP surveys of geometry such as for this study. One reason for completing p-wave analysis starting with depths below 600 ft. was because of raypath differences. (Other reasons were data quality deterioration and increasingly non-vertical p-wave incident angles.)

One can define a quantity Q, called "quality", which is related to ν and is independent of frequency in absence of dispersion:

$$Q = \pi / \nu V$$

Physically, Q is inversely proportional to wavelet broadening, and to the strain loss in energy per strain cycle:

$$Q = \Delta W / 2\pi W$$

W is work completed, and ΔW is energy lost. Q values for various rock types are given in Table 2.

Fluid saturation decreases both Q_p and Q_s, partly because fluids facilitate relative rock matrix motion along cracks, and also because motion of and absorption by the fluid itself causes some energy loss (Johnson et al, 1979). In a relative sense, Q_s is more affected by fluid saturation than Q_p. Gas saturation also decreases both quality parameters.

Taken together, Qs and Qp can help indicate the saturation characteristics of a reservoir. The question is whether in situ studies can provide resolution sufficient to isolate anelastic interval attenuation effects.

Processing Procedure

The Fortran software used for this study generated spectra from an interactively specified window of the

comparison waveforms. It calculated the logarithmic ratio of the spectra of the waveforms, and then yielded a plot of these spectral ratios. The user then picked the range over which to take a least-squares fit to determine ν. (See figures 24-27). This software was written by Marc Willis of M.I.T.

P-Wave Attenuation Analysis

The initial approach taken for processing the compressional wave data was to align the waveforms from all depths (accuracy was $\pm$1.5 ms, computed from high-resolution plots of each breaking waveform), and sum them over a desired depth interval, normalizing the output according to the number of traces in the stack. There were two motivations for stacking: to correct for source variability and to cancel reflection arrivals. The minimum stack size necessary to compensate for error introduced by these source and reflection problems was found to be about 150 ft., which is close to the dominant compressional wavelength of about 190 ft. Attenuation over smaller intervals was less than experimental error.

Stacking did not completely destroy the effects of reflection arrivals. Ganley and Kanasewich (1979) discuss the effect of reflection arrivals on attenuation computations. Reflections, like primary arrivals, experience anelastic attenuation, so that complete cancellation due to destructive interference incurred by stacking is not possible. Nevertheless, summation does greatly reduce the effects

of reflections.

Source consistency was a major concern. Major elements of the source problem included variation in thumper ramp acclivity, and coupling problems introduced by each thumper reorientation and each addition of dry cement. Extreme shot-to-shot source variations were identifiable by means of inspection of the trends in monitor geophone versus downhole geophone arrival strengths. The data was run through a Fortran program which flagged those depths where the energy arriving through a compressional wave window was markedly different from that coming in at nearby depths and from that arriving at the same depth from the thumper set at the opposite polarity. Where amplitudes were anomalous on both downhole and monitor geophones, that depth point was removed from the stack. In this way, five depth points were removed from the section for each thumper polarity.

A much more difficult problem was variation in source strength due to cumulative effects. It was not random, so stacking did not cause any cancellations. Rather, the frequency content of the source waveform increased consistently over time, and equivalently, as the geophone moved uphole. This was probably due to general compaction of the ground near the source. Figure 21 shows monitor geophone vertical component spectra which correspond to the shots for the indicated stacks of eastward downhole traces. The shift in frequency content was greatest at the beginning of the survey, and by the time the geophone had moved up to a depth

of 1,100 feet the frequency content of the waveform reaching the monitor geophone had almost stabilized.

The frequency shift was probably caused more by alterations in the coupling between source and ground than by a change in character of the source itself. This made the task of monitor phone calibrations difficult, because the monitor and downhole geophones sensed different parts of the source's radiation pattern, and the quality of the couple probably varied spatially as well as over time. Nevertheless, the only possible correction was to incorporate information from the monitor geophone with that from the downhole arrivals.

The correction technique used assumed that the spectral amplitudes of the vertical component of the monitor geophone corresponded directly to those of the comparison source waveforms, A_1^S and A_2^S. After correcting for spherical spreading, the amplitudes at a certain depth and time can be written as:

$$A(z_1)=A_1^S(e^{-\alpha z_1})$$

$$A(z_2)=A_2^S(e^{-\alpha z_2})$$

Then

$$\frac{A(z_2)}{A(z1)}=\frac{(A_2^S)}{A_1^S}(e^{-\alpha(z_2-z_1)}$$

Removal of source variation effects was then done by cancelling (A_2^S/A_1^S): the algorithm multiplied the deeper downhole spectrum by the monitor spectrum for the shallow stack, and the deep monitor spectrum by the shallow downhole spectrum. This correction was completed for those (deeper)

stacks for which frequency shift was significant.

The spectral ratio method used had significant limitations. Inaccuracy of Q measurements increases as the Q increases, and the slope of the natural logarithm of the spectral ratios of the traces of interest decreases. Noise begins to dominate in these cases. Also, in such instances, the Q value computed is significantly affected by the choice of the spectral window for attenuation computation. Windows chosen for the listed values were picked for spectral ranges where compressional wave energy was strongest, and covered a frequency band centered near 30 Hz, with a width of about 16 Hz.

An example of the effects of spectral window size variation is the monitor-corrected comparison, for 150-foot stacks, of the arrivals centered at 975 and 1,125 feet, for which the Q goes from -28 to 700 to 80 as the window widens. (the value of 80 was picked with a typical window width of 22-39 hertz, while the first two values were for narrow windows which excluded some frequencies with strong amplitudes). In cases such as this, attenuation is probably low, within the range of experimental error. It is possible in this case that monitor geophone corrections overcompensated for downhole source radiation patterns, or that constructive interference strengthened the deeper waveform.

Time window length of the comparison waveforms can also influence calculations. Tests showed that too short a window yields a spectrum dominated by the properties of the

sine taper used to prepare the trace for spectral analysis, while too long a window includes more interference effects. Time windows used for the compressional wave analysis discussed here were all four cycles long.

Results for Q_p

Tables 3-5 show values of Qp computed from 150-and 200-foot stacks of the vertical component of the downhole geophone. Figures 22 and 23 are plots of the spectra for compressional waveforms which were sums of fifteen traces whose depths were centered on the indicated depths.

One result immediately stands out, that being that attenuation is markedly higher across that zone including the main gas sand. Elsewhere, values for Qp show notable variability, as one value is negative, while other values are relatively high.

Nevertheless, comparison of Q values computed shows a rough correspondence between the values for stacks from the thumper with eastward versus westward orientation. As discussed in the geologic section, lithology from the depths of 600 to about 1,320 feet consists mainly of shaly strata with small sandy and silty layers interspersed. Attenuation is moderate through the shallowest shale layers, and decreases with depth and compaction. Q values vary from 12 to 85, but center around 35, with four of the eight data points within 10 of that value. In the region around the larger gas zone, Q values for both sources drop dramatically to about 2, and

then diverge to -15 and 5 for east and west sources, respectively, for the next interval.

Q values computed after monitor phone corrections show greater east-west skew, but qualitatively indicate, again, intermediate attenuation in the shallower shales, reduced attenuation through the deeper shales, high attenuation in the region of the gas zone at 1,320 feet, and moderate attenuation in the lowest zone which includes the second gas zone and a high-velocity shale. The most anomalous Q values are for the stacked arrivals centered on 975 versus those centered on 1,125, where both Q's are close to -30. Perhaps monitor geophone corrections incorrectly compensated for source frequency shifts in these regions, or perhaps constructive interference affected the deeper waveform. The high negative and high positive Q values for east and west stacks about 825 versus 975 ft. represent only small differences in a very flat slope centered about zero; both indicate very small attenuation, in the range of experimental error.

More measurements, for 200-foot stacks, compared the region just above the gas sand to that zone including and below the gas, and they also indicated high attenuation through the region including the gas. Q values were about 2 before source variation corrections, while compensated values centered on 5. Figures 24-27 show the spectral windows and associated log ratio plots used for these determinations.

Shear Wave Attenuation

Processing

The shear wave (primarily SH) arrivals were received mainly on the two horizontal components of the downhole geophone, and their preferred horizontal polarity was perpendicular to the line from the thumper to the well. But since the downhole geophone continually re-oriented itself as its cable twisted during each relocation, the horizontal components of the geophone needed to be artificially re-oriented in order to isolate the SH-arrivals consistently on one channel. The rotation algorithm operated according to the assumption that the energy arriving within a user-specified time window was primarily shear. The program iterated through 180° in 1° steps, and chose that rotation angle which maximized shear energy arriving at the designated channel. This channel, the SH-maximized record, will be referred to as the transverse trace.

Figure 5 shows the three components of the downhole geophone at a depth of 1500 ft. The transverse channel has a greater amount of shear energy, and less compressional wave energy, than the other rotated horizontal channel.

A problem with the rotation algorithm was that, depending on real downhole geophone orientation, it chose either the correct polarity of the shear arrival or its reverse. The best in-stream correction is to compare the rotated

waveform with a previously rotated arrival having the correct polarity.

A comparison of east with west shear wave rotation angles for the same depth point (fixed geophone) showed that the computed rotation angles usually ranged over $\pm 15°$. Variation was due in part to limitations of the rotation algorithm, but real differences in source realignments could also have contributed to variations.

The rotation algorithm was effective when incident energy was indeed primarily shear, and compressional reflection and tube wave interference was minimal. Careful, trace-by-trace, rotation window selection largely alleviated the interference problem, but further processing was completed in order to correct for small rotation differences caused by contamination.

The first step in the rotation correction procedure was to align all of the horizontal traces according to the shear wave arrival times (picked to ± 3 ms). Alignments were next fine-tuned by computer, and the rotation calibration sequence began. Starting with the deepest traces (least likely to be contaminated by tube waves), the SH arrival at each depth point was compared to a summed composite of three previously re-rotated SH arrivals from points directly below it, and was then re-rotated through ± 15 degrees in order to maximize the semblance between it and the reference stacked trace.

Once rotation, alignment and rotation calibration were

completed, the transverse, traces were summed over 400-foot intervals. A stack was again necessary in order to account for possible shear wave reflections, other wave-type contamination, and source variations. Attenuation measurements were tried for a variety of window lengths, and finally a two-cycle window was chosen as a compromise between desire for as much shear arrival information as possible and need to minimize depth-dependent interference effects. Figure 29 shows the impact of a larger window size of seven cycles, versus a more typical length of four periods.

Nevertheless, interference was still a problem. Although simple analog trace analysis indicated that the primary frequency was about 20 Hz, the spectra from the two-cycle windows showed a bimodal spectral distribution with humps around ten and thirty hertz, and a node at 20 Hz. Attenuation calculations were then made using two methods: with a short spectral window about the 10-Hz hump, and with a much longer window including both humps.

Qs Results

Table 6 shows the results of shear wave attenuation measurements calculated over a series of intervals. East- and west-thumper orientation SH-sections were analyzed separately, as for compressional waves, and results showed rough correlation between the Q's found for each polarity. Attenuation of the shear waves was consistently greater than

for compressional waves, as Q's values ranged from a minimum of 10 to a maximum of 50. Six of the ten Q values tabulated were closely spaced about 11, and the high Q's are all for narrow spectral windows (centered about 10 hertz).

Source waveform variability, geophone ring, and interference combined to make the shear wave spectra variable over depth, so a check was run using two smaller stacks centered about 810 and 1,200 feet, including approximately twenty of the best data points from the west section. Q values computed from comparison of those stacks agreed roughly with previous runs. For a short spectral window (5-15 hz), Q_S was near 15, and for a long spectral window (5-30 hz), Q_S was about 25. (See figure 30 for the spectral and log ratio plots for these stacks.

Conclusions

A vertical seismic profile was completed in order to investigate the seismic properties of shallow Gulf Coast sediments. The experimental equipment generated both compressional and shear wave data, from which velocity and attenuation determinations were made.

Use of 10 ft. clamping offsets downhole was sufficient to constrain compressional wave attenuation measurements to intervals of about a wavelength, and velocity calculations to zones of one-half wavelength. The dominant p-wave wavelength was 190 ft., and the average V_p was 6070 ft/s. Shear waves, with a dominant wavelength of about 90 ft. and velocities averaging 1540 ft/s, one-fourth of the p-wave velocities, had potential for greater spatial resolution, but source consistency problems increased the minimum interval size for attenuation calculations.

Analysis of well-log data enabled the investigator to divide strata into four sediment classes. A straight-raypath, two-dimensional raytracing program was then used to generate a velocity structure which yielded the following sediment velocity relationships:

for the near-surface, V_p was 4860 ft/s, while V_s was 700 ft/s;

for sands, V_p was 5960 ft/s, and V_s was 1300 ft/s;

for silts, V_p was 6075 ft/s, while V_s was 1430 ft/s;

and for shaley clays, V_p was 6050 ft/s, and V_s was

1710 ft/s.

However, the dominant factor affecting velocities was compaction. Both p-and s-velocities increased consistently with depth, though shear velocities were more strongly altered with burial depth.

Through the gas zone, p-wave velocities dropped significantly, while s-wave velocities were not changed as much. This result was apparent from both ray-tracing modelling and sonic log measurements.

Attenuation measurements were completed after a processing sequence which aligned traces from all depth points and then summed them over depth intervals of interest. Shear wave processing included the additional steps of artificial geophone rotation using an energy-maximization technique for a shear wave window, and re-rotation using semblance methods.

Both p-and s-waves traces were checked by a program which flagged shots for which arrivals exhibited anomalous arrival strength.

Another kind of source variation, involving a continual increase in signal frequency content due to a change in the source-ground couple over time, required monitor geophone calibrations. The following results are for data to which this series processing steps had been applied.

Q_p values centered about 35, but ranged from a maximum of 90 to a minimum of 5. As the geophone passed

through the major gas sand, Q_p dropped significantly, to about 5, even after monitor geophone corrections were added. Q_p values were highest in the intermediate depth shales (40), and were less large through the shallow shales and that layer including both the deeper gas zone and deepest shales (25).

Average Q_s was about 25. Q_s showed smaller variation with depth and source orientation than did Q_p. Interference effects, probably due to near-surface multiples, caused some frequency-dependant variations in attenuation.

Recommendations

More study is needed to determine the radiation patterns of the source. This will constrain attenuation measurement error with respect to time (source variations) and depth (spacial variations). In particular, the relationship between monitor geophone and downhole signal strengths needs to be resolved.

Use of a source with stationary baseplates might help to improve source consistency. Deeper burial of the monitor geophone will help to increase confidence in monitor geophone corrections.

Acknowledgements

I would like to thank Dr. Bob Lucas at Amoco Production Research Company for providing assistance and support for this study. Also, my special thanks to Lana Nelson at Amoco Production Company in New Orleans for her patience and kindness in helping this fledgling programmer in his first encounters with that awful monster called CMS. Bob Melton was a great help in interpretation of the geology from the well log data, and Dr. Jeff Johnston, my advisor at Amoco, was a valuable source of information and advice.

At M.I.T., Dr. Roger Turpening and Robert Stewart were invaluable in generating ideas, approaches, and encouragement. Marc Willis provided the Fortran software which was used for attenuation analysis. Pam Stanley assisted with velocity analysis, and Paul Cunningham didn't.

Especially, I would like to thank Professor Toksoz for his recommendations, support and understanding. I was very lucky to meet him through field camp in 1979; I believe that he likes eggnog almost as well as lard bread.

Finally, my thanks to my bro's, who embody the eternal essence of ROGS.

References

Aki, K. (1976) Signal to noise ratio of seismic measurements, Volcanoes and tectonosphere, edited by Hitoshi Aoki and Susumu Iizuku, Tokai University Press.

Anderson, D. L., et al., Attenuation of seismic energy in the upper mantle: J. Geophys. Res., 70,1441-1448, 1965.

Auberger, M. and J. S. Rinehart, Method for measuring attenuation of ultrasonic longitudinal waves in plastics and rocks: J. Acoust. Soc. A., 32, 1698-1699, 1960.

Birch, F. and D. Bancroft, Elasticity and internal friction in a long column of granite: Bull. Seis. Soc. Amer., 28, 243-255, 1938.

Born, W. T., The attenuation constants of earth materials: Geophysics, 6, 132-138, 1941.

Collins, F. and C. C. Lee, Seismic wave attenuation characteristics from pulse experiments: Geophysics, 21, 16-40, 1956.

Dix, C. H., The Interpretation of well-shot data, Geophysics 10, 2, 160-170, 1945.

Gal'perin, E. I., Vertical Seismic Profiling, Society of

Exploration Geophysicists Special Publication No. 12, Tulsa, Okla., 1974.

Ganley,D.C., and Kanasewich,E.R., Measurement of absorption and dispersion from check-shot surveys: Institute of Earth and Planetary Physics, University of Alberta, Edmonton, Alberta, Canada,1977.

Gardner,G.H.F., Wyllie,M.R.J., and Droschak,D.M., Effects of pressure and fluid saturation on the attenuation of elastic waves in sands: J. Petroleum Technology, p.189-198,1974.

Gordon, D. H. , Velocity and attenuation in imperfectly elastic rock: J. Geophys. Res., 73, 3917-3395, 1968.

Horton, C. W., A loss mechanism for Pierre shale: Geophysics 24, 667-680, 1959.

Johnston, D. H., The attenuation of seismic waves in dry and saturated rocks: Ph.D. Thesis, MIT, Dept. of Earth, Space ond Planetary Sciences,1978.

Johnston, D. H., Toksoz,M.N., and Timur,A., Attenuation of seismic waves in dry and saturated rocks, Part II, Toeoretical models and mechanisms, Geophysics, 44, p.691-711,1979.

Kennet,P., Ireson,R.L., and Conn,P.J., Vertical sesimic profiles and their application in exploration

geophysics: Geophisical Prospecting, p. 676-699,1980.

Knopoff, L., Q:Rev. Geophys., 2, 625-600, 1964.

Kuster, G. T., Toksoz, M.N. (1974) Velocity and attenuation of seimic waves in two-phase media: Part I and Part II, Geophysics, 39, 587-618.

Lash, C. C., Shear waves, multiple reflections, and converted waves formed by a deep vertical wave test (vertical seimic profiling), Geophysics, 45, 9, 1373-1411, 1980.

McDonal, F. J. et al., Attenuation of shear and compressional waves in Pierre shale, Geophysics, 23, 3, 421-439, 1958.

O'Brien, P. N. S. , A discussion on the nature and magnitude of elastc absorption in seismic prospecting: Geophys. Prosp., 9, 261-275, 1961.

Pelesnick, L. and I. Zietz, Internal friction of fine grained limestones at ultrasonic frequencies: Geophysics, 24, 285-296, 1959.

Ricker, N., The form and laws of propagation of seismic wavelets: Geophysics, 18, 10-40, 1953.

Schoenberger,M., and Levin,F.K., Apparent Attenuation due to intrabed multiples,II: Geophysics,43,730-737,1978.

Strick, E., The determination of Q, dynamic viscosity and transient creep from wave propagation measurements: Geophys. J. Roy. Astro. Soc., 13,197-218, 1965.

Stewart, R. R., R. M. Turpening, and M. N.Toksoz, Study of a subsurface fracture zone by vertical seismic profiling, submitted for publication in Geophysical Research Letters, 1981.

Toksoz, M. N., R. M. Turpening, and R. R. Stewart, Assessment of the Antrim Oil Shale fracture zone by seismic profiling, U. S. Dept. of Energy Report No. FE-2346-91, September, 1980.

Toksoz, M. N., Johnston, D.H., and Timur, A., Attenuation of seismic waves in dry and saturated rocks, Part I, Lab measurements, Geophysics, 44, p.681-690, 1979.

Tullos,F.H., and Reid,A.C., Seismic attenuation of gulf coast sediments: Geophysics,34,516-528,1969.

Walsh, J. B., Seismic wave attenuation in rock due to friction: J. Geophys. Res. 71, 2591-2599, 1966.

White, J. E., "Seismic Waves: Radiation, Transmission, and Attenuation", McGraw-Hill, NY, 1965.

Wuenschel, P. C., Dispersive body waves-an experimental study: Geophysics, 30, 539-551, 1965.

Figures

1. Survey geometry.

2. The thumper source with weight ramp in its three primary configurations. The bottom two positions were used in this survey (from Toksoz et al, 1981).

3-4. Geologic section.

5. Waveform arrivals recorded on the three components of the downhole geophone for a depth of 1500 ft. Horizontal traces shown were rotated during processing in order to isolate shear wave energy on the trace displayed uppermost here.

6-9. Arrivals to the vertical component of the downhole geophone for the depths indicated.

10. Overlay plot of the transverse, or shear wave-maximized trace for the thumper source in east and west configurations, from the downhole geophone at 1,500 feet. Compressional arrivals break with the same polarity, but shear waves come in with reversed first particle motions, due to source reorientation.

11-16. Shear wave traces. These waveforms were computed by subtracting corresponding transverse records for the thumper source in east and west orientations. Since for different polarities signals retain the same polarity for compressional waves, but reverse polarities for shear waves,

this subtraction technique enhances shear wave arrivals. The traces were calibrated for variations in p-wave arrival strength with source reorientation before subtracting. Scaling was done over a p-wave window around the time of first-break p-arrivals.

17. First arrival times for compressional and shear waves as a function of depth.

18. Plot of compressional, shear, and sonic log velocities with depth. The two former velocity structures were computed using a flat-layer ray tracing program.

19. The ratio between compressional and shear wave velocities as a function of depth. Shear wave velocities increase relatively quickly with depth.

20. Travel time residuals for the sonic log velocity model. Inputs were averaged sonic velocities. The residuals are the difference between computed and real times. The error range for p-wave travel time picks is about 2 ms. Sonic model travel times are significantly greater than real travel times for shallow depths.

21. Amplitude spectra for sums of arrivals at the vertical components of the monitor geophone during a compressional wave time window. The stacks are for source shots for which the downhole geophone was positioned as indicated.

22. Amplitude spectra for first compressional wave

arrivals received on the vertical component of the downhole geophone for clamping depths centered on the indicated values. All arrivals were from the thumper source in its eastward orientation.

23. Downhole geophone compressional spectra as in figure 22, but received from the thumper in its westward orientation.

21-24. Plots of the compressional wave first arrival spectra, and the ratio of the natural logarithms of the amplitude coefficients for each frequency, for stacks of vertical downhole geophone traces centered on 1260 and 1410 feet (including clamping points from 1,200 to 1310, and 1320 to 1510 feet,respectively). The main gas zone was at 1,320 to 1,340 feet. Chosen spectral window limits are marked with arrows.

Figures 24 and 25 are for arrivals which had not been corrected for source variations.

Figures 26 and 27 show source-corrected spectra. Attenuation decreased with the corrections, but was nevertheless hogher than through any other section of strata near the well.

28. P-wave Q-values. These calculations are averages for east and west orientations. Monitor-phone calibrated values were used for the deepest intervals.

29. A comparison of shear wave spectra for different time

windows, of seven and four cycles, starting with first shear wave arrivals. Interference is greater for longer windows.

30. A sample spectral comparison for two shear wave stacks centered on 810 and 1200 feet. Attenuation was calculated for both short (usually 5-14 hz) and long (5-30 hz) shear wave windows. Interference destroyed much of the arriving signal near 20 hz.

Tables

1. Velocity relationships between compressional and shear waves computed for three sediment classes determined from well log analysis.

2. Q values for various rock types. From Johnston (1978).

3-5. Computed Qp values for 15-member sums of waveforms arriving to the vertical component of the downhole geophone for clamping levels distributed about the indicated average depths.

Figure 3 shows computations found without source corrections.

Figure 4 shows calculations with source corrections, as determined from the monitor geophone arrivals.

Figure 5 gives Qp values found for the indicated sums of traces just above and just below the primary gas zone.

6. Computed Q_S values for the indicated intervals.

Appendix 1

Equipment Description

The seismic source used for the analysis of this paper was a gravity weight-drop device known as a "thumper". Figure 1 shows the thumper in various configurations. For the tests run on the Gulf Coast, the thumper operated with the weight ramp in the two non-vertical orientations.

The weight used was 1500 pounds, and it slid down an eight foot long ramp which was inclined 45° from the horizontal. The weight's maximum extension was nine feet from its base, protruding one foot above the ramp's end. The force of impact was distributed by a 2 ft. square metal base plate at the ramp's base. Whenever the thumper changed orientations it also moved the baseplate, and the operator tried to minimize the resultant coupling changes by running a few test shots.

Both monitor and downhole geophones had three mutually perpendicular components. Signals arriving at the geophones were recorded by Minie-Sosie instruments on two banks with gains 12 db apart. The sampling rate used was 2 milliseconds, and the total listening period was two seconds.

A vacuum-driven weight drop machine and a shear-wave vibroseis truck operated in addition to the thumper, but only for 100-foot downhole geophone spacings.

In addition, a surface geophone array was also used to record the arrivals from the vibroseis source. The data from these sources was not used for the discussion in this paper.

```
      dimension vel(165),angle(1650)
      dimension trav(165),level(1650),thick(165),trtime(1650)
c
c          vel is the array of velocity values
c          thick is an array with interface depths.
c          nlay specifies the number of layers in the model
c          Thetai is the initial angleof the initial ray for raytracing
c               iterations.  It and all other angular
c               information is measured from the vertical.
c          Thetaf is the last angle for raytracing iterations.
c          Thiacr is the increment between incident angles for
c               successive iterations.
c          Walk is the source-to-well offset.
c     zmax is the survey bottom depth
c          incr is the offset between real geophone
c               clamping depths
c
c          level is an array storing depths at which rays are incident.
c          angle is an array storing initial incident angle info.
c          trtime is an array storing travel time values.
c          This is Jenny Caldwell Memorial fortran.
c
c          The program traces rays from a succession of incident
c          angles controlled by the user.  It records the depth at
c          which the rays arrive at the well as well as their travel
c          times, and interpolates to find travel times at depths
c          for which there are real travel time measurements.
c          The program stores these travel times, and the user can
c          input them into a residual comparison program
c          of his liking.  Interpolation becomes inaccurate when
c          ray offsets are very large.  The program records the
c          maximum interval between ray arrivals, and also stores
c          arrival information for the user to inspect to decide
c          if he needs a smaller angular increment.
c
      zmax=1650.
      walk=261.
      incr=10
      character response
      write(6,1)
    1 format(' enter 1 if you want structure parameters read from file')
      read(5,2) iread
    2 format(i)
      write(6,17)
   17 format(' enter number of layers')
      read(5,2) nlay
      if(iread.ne.1) go to 3
      call read(thick,vel,nlay)
c
c          Subroutine read reads in velocity structure values
c          from storage files.
c
      go to 4
    3 do 10 mm=1,nlay
      write(6,5) mm
    5 format(' layer',i5)
      write(6,6)
    6 format(' enter layer thickness')
      read(5,2) thick(mm)
      write(6,8)
    8 format(' enter layer velocity')
```

```
      read(5,2) val(mm)
   10 continue
    4 write(6,11)
   11 format(' enter thetai')
      read(5,2) thetai
      fac=.01743589
      thetai=fac*thetai
      write(6,13)
   13 format(' enter thetaf')
      read(5,2) thetaf
      thetaf=fac*thetaf
      write(6,15)
   15 format(' enter angle increment')
      read (5,2) thincr
      thincr=fac*thincr
      nlast=((thetaf-thetai)/thincr)+1.
      theta=thetai
      j=1
      do 20 kk=1,nlast
      trtime(j)=0.
      xtot=0.
      dis=0.
      ztot=0.
      thnew=theta
      angle(j)=theta/fac
      do 30 ll=1,nlay
      dx=thick(ll)*tan(thnew)
      xint=xtot+dx
      if(xint.ge.walk) go to 31
      xtot=xint
      depth=ztot+thick(ll)
      if(depth.gt.zmax) go to 34
      ztot=depth
      dis=thick(ll)/cos(thnew)
      delt=dis/val(ll)
      trtime(j)=trtime(j)+delt
      tain=(val(ll+1)/val(ll))*sin(thnew)
      if(tain.gt.0.9999) go to 35
      thnew=asin(tain)
   30 continue
   31 x=walk-xtot
      dx=x/tan(thnew)
      level(j)=ztot+dx
      dis=x/sin(thnew)
      delt=dis/val(ll)
      trtime(j)=trtime(j)+delt
      j=j+1
      go to 34
   35 nlay=ll
   34 theta=theta+thincr
      if(theta.gt.1.5707863) go to 42
   20 continue
      go to 41
   42 ii=j
      m=j-1
      go to 43
   41 ii=j+1
      m=j
   43 trtime(ii)=walk/val(1)
      level(ii)=0.
      angle(ii)=0.
```

```
      mr=0
      ii=0
      do 112 n=1,ii
      write(7,110) level(n),trtime(n),angle(n)
  110 format(' n=',i6,' trtime=',f12.5,' incident angle=',f12.5)
      ii=level(n)-level(n+1)
      if(ii.lt.max) go to 112
      max=ii
      mr=n
  112 continue
      write(6,113) max,angle(mr+1),angle(mr)
  113 format(' zmax=',i5,' between angle=',f12.5,' and',f12.5)
c
c          Now for interpolation
c
  638 do 70 k=1,165
      k10=k+incr
      do 80 m=1,ii
      if(k10.eq.level(m)) go to 85
      if(k10.gt.level(m)) go to 79
      r=level(m)-level(m+1)
      p=trtime(m)-trtime(m+1)
      trav(k)=(p/r)*(k10-level(m+1))+trtime(m+1)
      go to 69
   79 m=m-1
      if((level(m).eq.0).and.(k10.gt.10)) go to 81
   80 continue
   81 write(6,830) k10
  830 format(' no rays arrived below',i6,' feet')
      go to 71
   85 trav(k)=trtime(m)
   69 continue
   70 continue
   71 continue
      do 260 i=1,k
      i10=10*i
      write(4,261) i10,trav(i)
  261 format(i7,f12.5)
  260 continue
      stop
      end
c
c
c
      subroutine read(thick,vel,n)
      dimension jdeep(165),vel(165),thick(165)
      read(3,8) jdeep(1),vel(1)
      thick(1)=jdeep(1)-0
      if(n.eq.1) go to 11
      do 10 i=2,n
      read(3,9) jdeep(i),vel(i)
    9 format(i7,f12.5)
      thick(i)=jdeep(i)-jdeep(i-1)
   10 continue
   11 return
      end
```

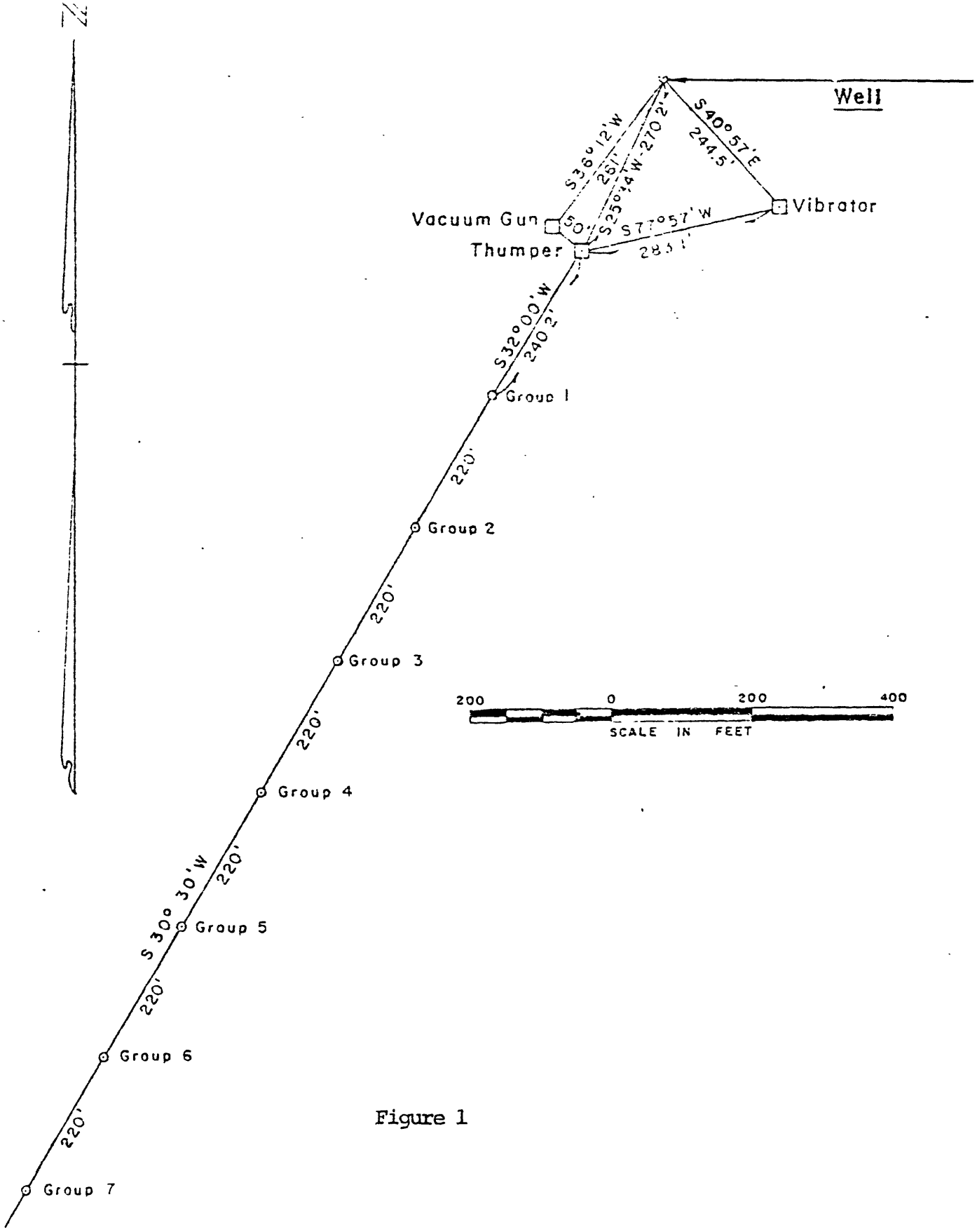
Well
S36°12'W
251'
S25°14'W-270.2'
S40°57'E
244.5'
Vacuum Gun
50'
Thumper
S77°57'W
285.1'
Vibrator
S32°00'W
240.2'
Group 1
220'
Group 2
220'
Group 3
220'
Group 4
S30° 30'W
220'
Group 5
220'
Group 6
220'
Group 7
200
0
200
400
SCALE IN FEET

Figure 1

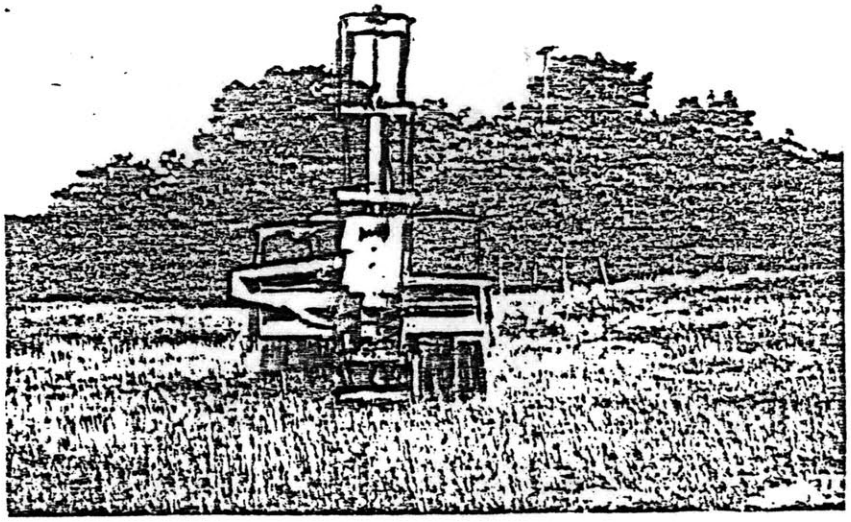

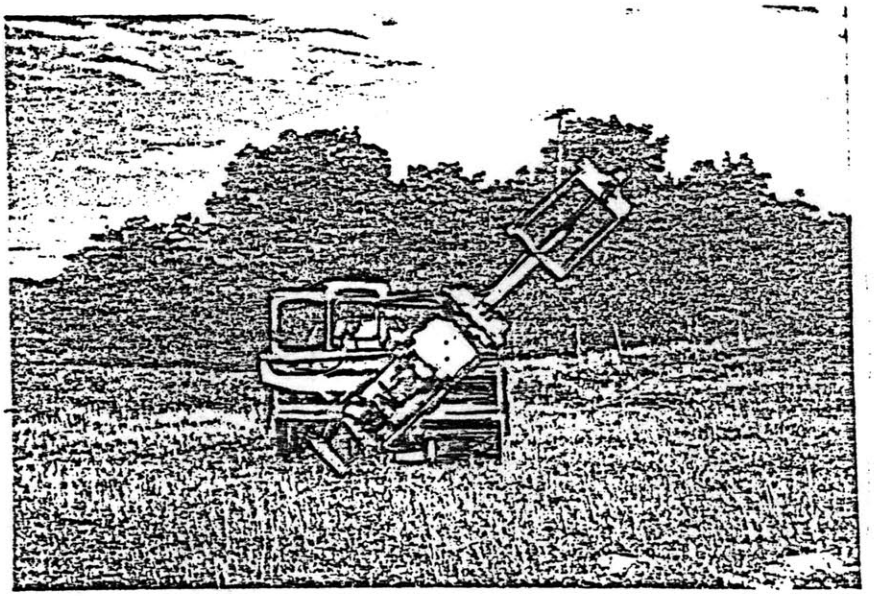

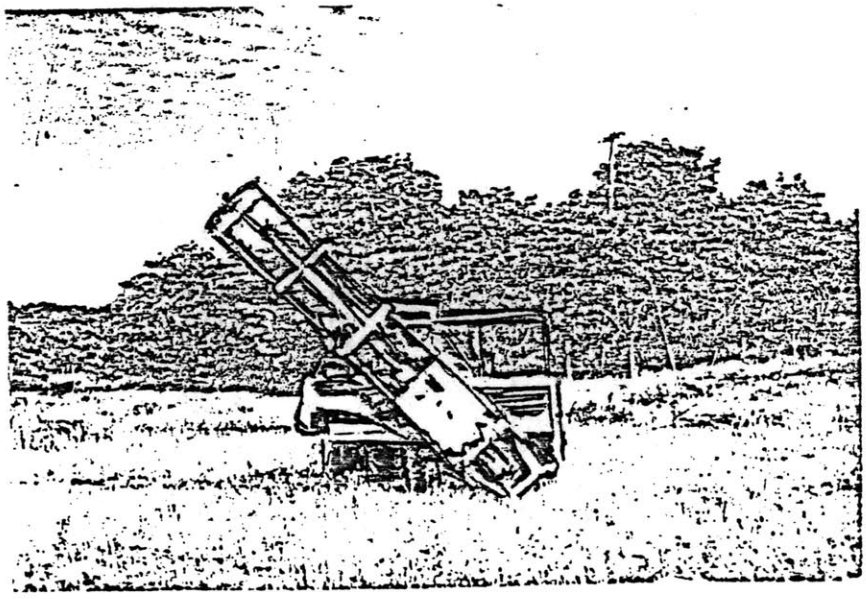

Figure 2

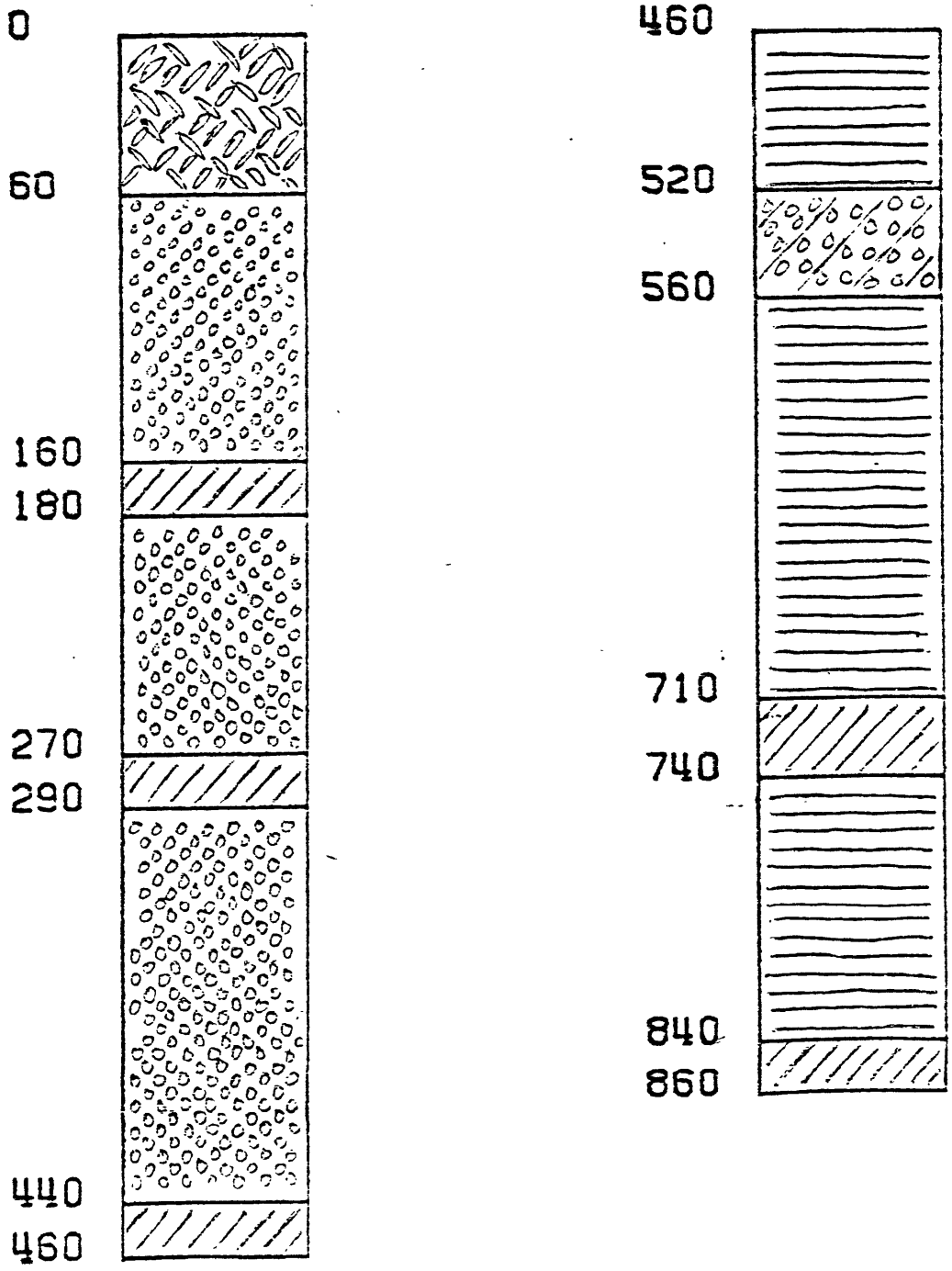

Figure 3

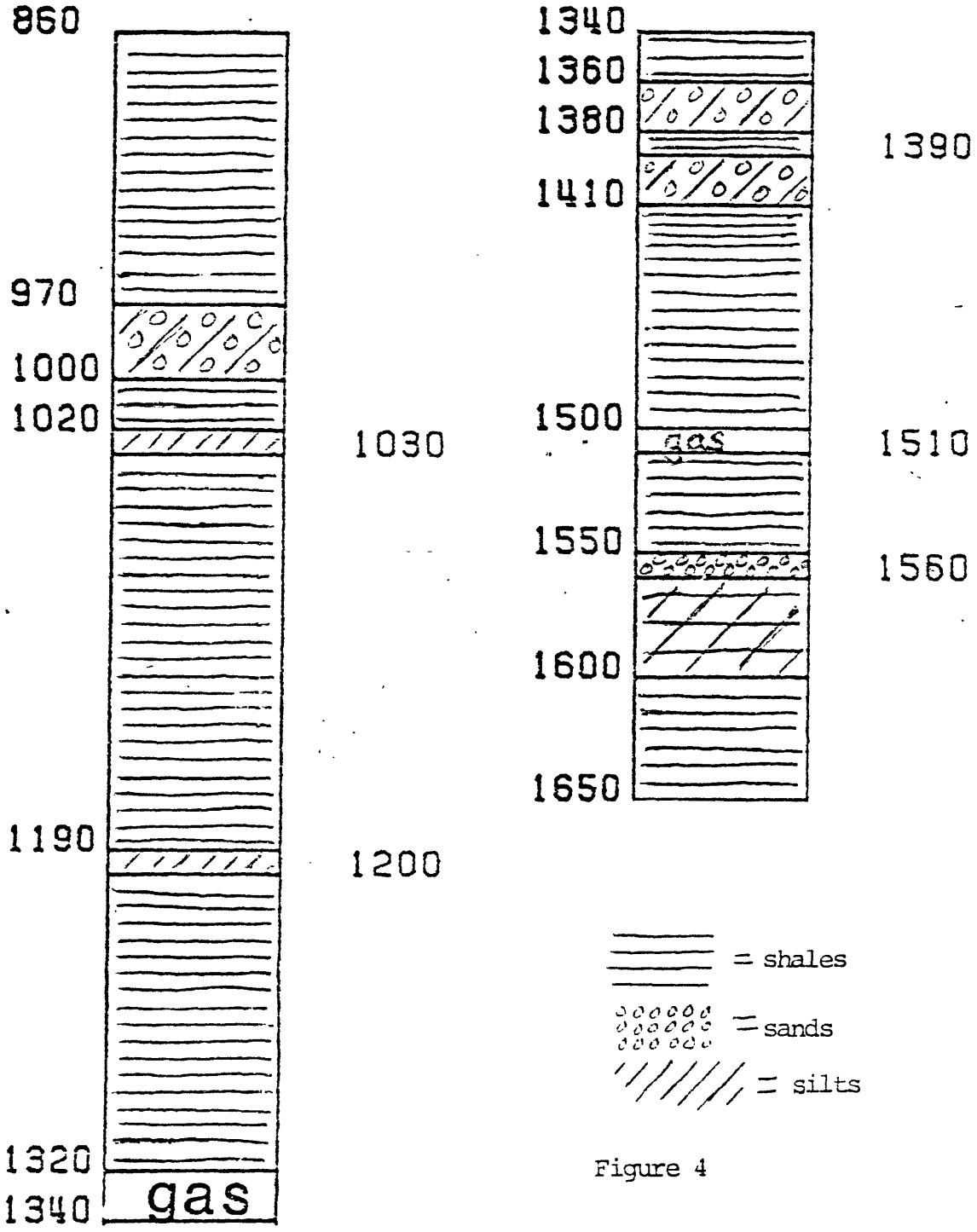
860
970
1000
1020
1030
1190
1200
1320
1340
gas
1340
1360
1380
1390
1410
1500
gas
1510
1550
1560
1600
1650
= shales
= sands
= silts

Figure 4

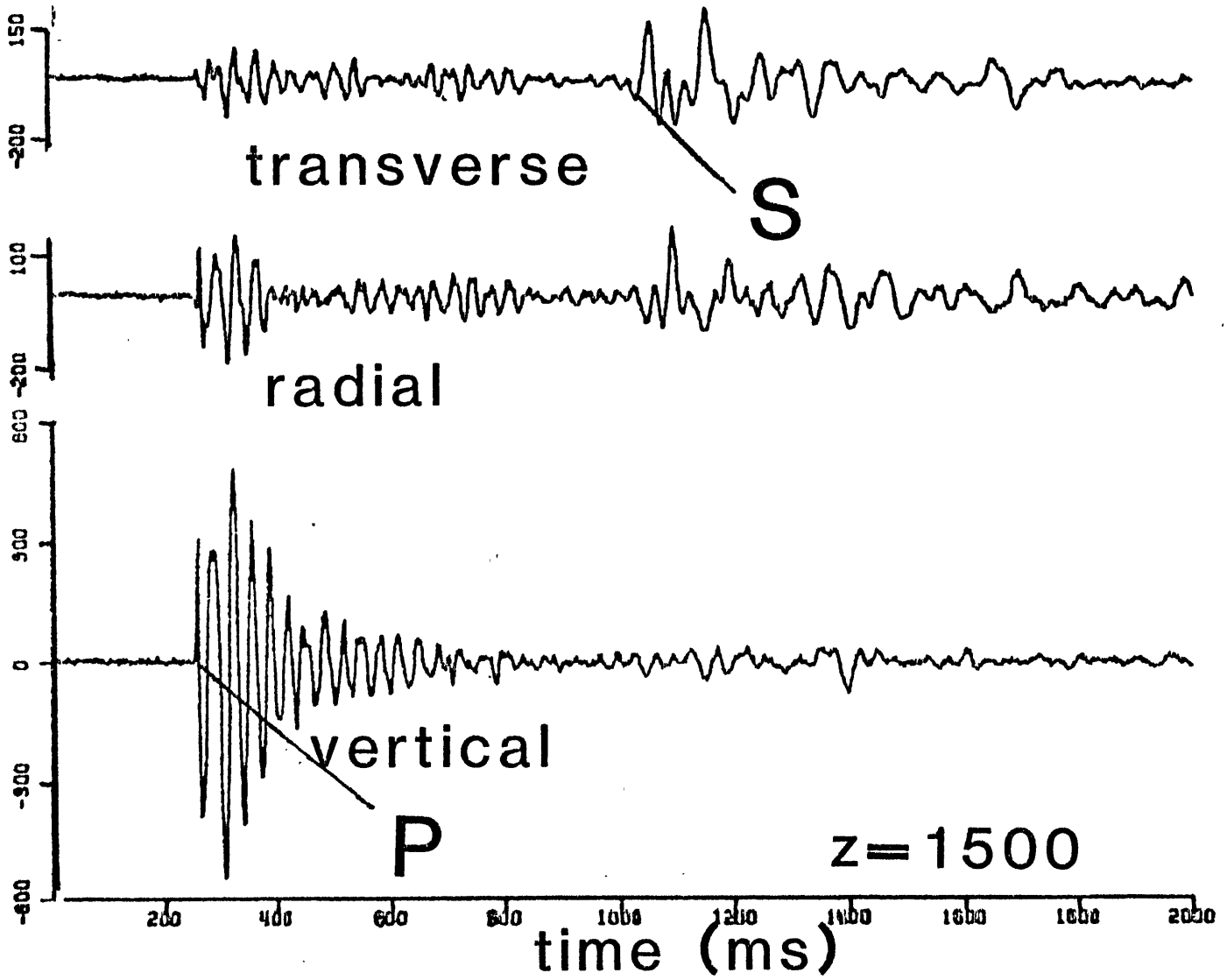

Figure 5

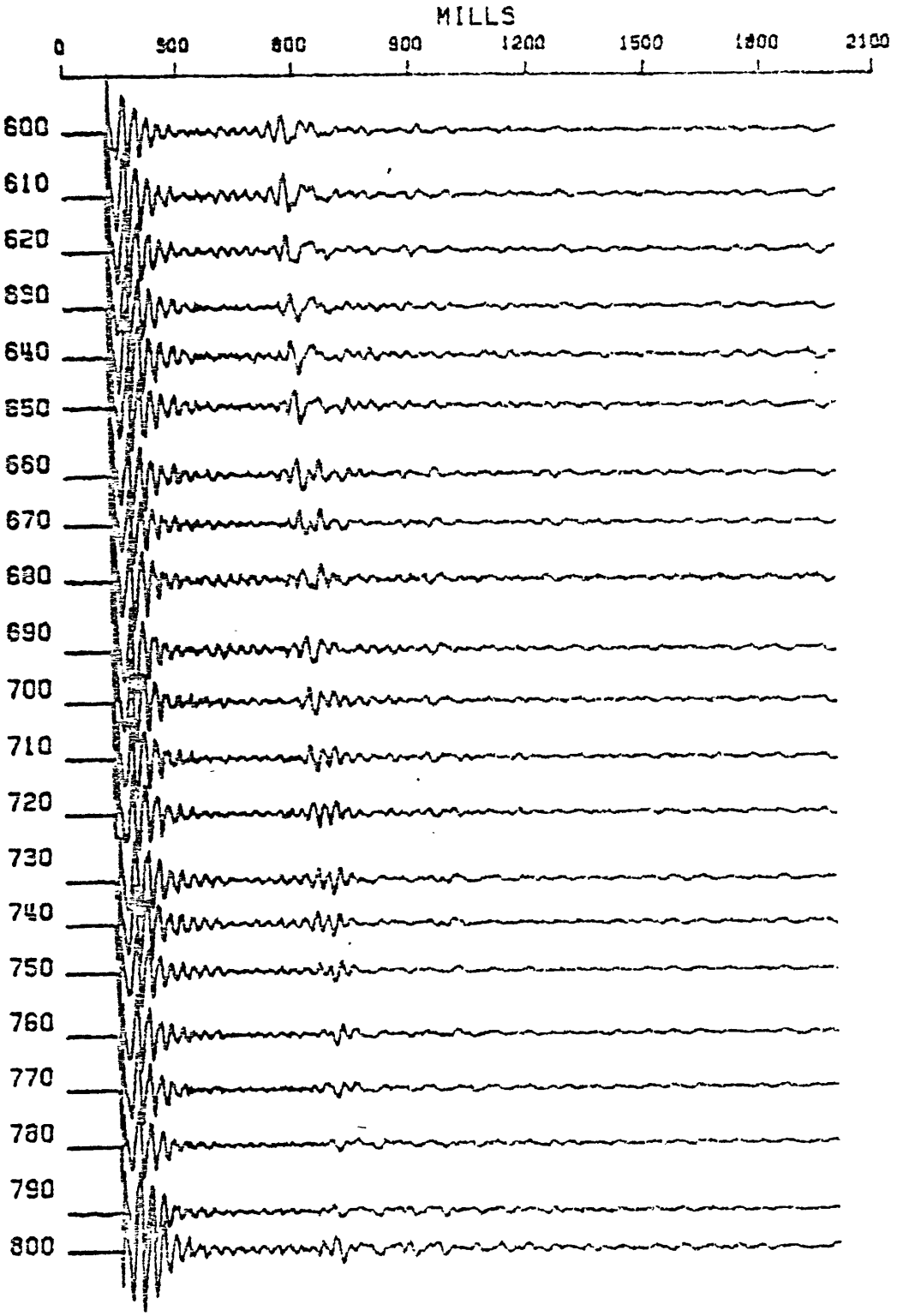
MILLS
0
300
600
900
1200
1500
1800
2100
600
610
620
630
640
650
660
670
680
690
700
710
720
730
740
750
760
770
780
790
800

Figure 6

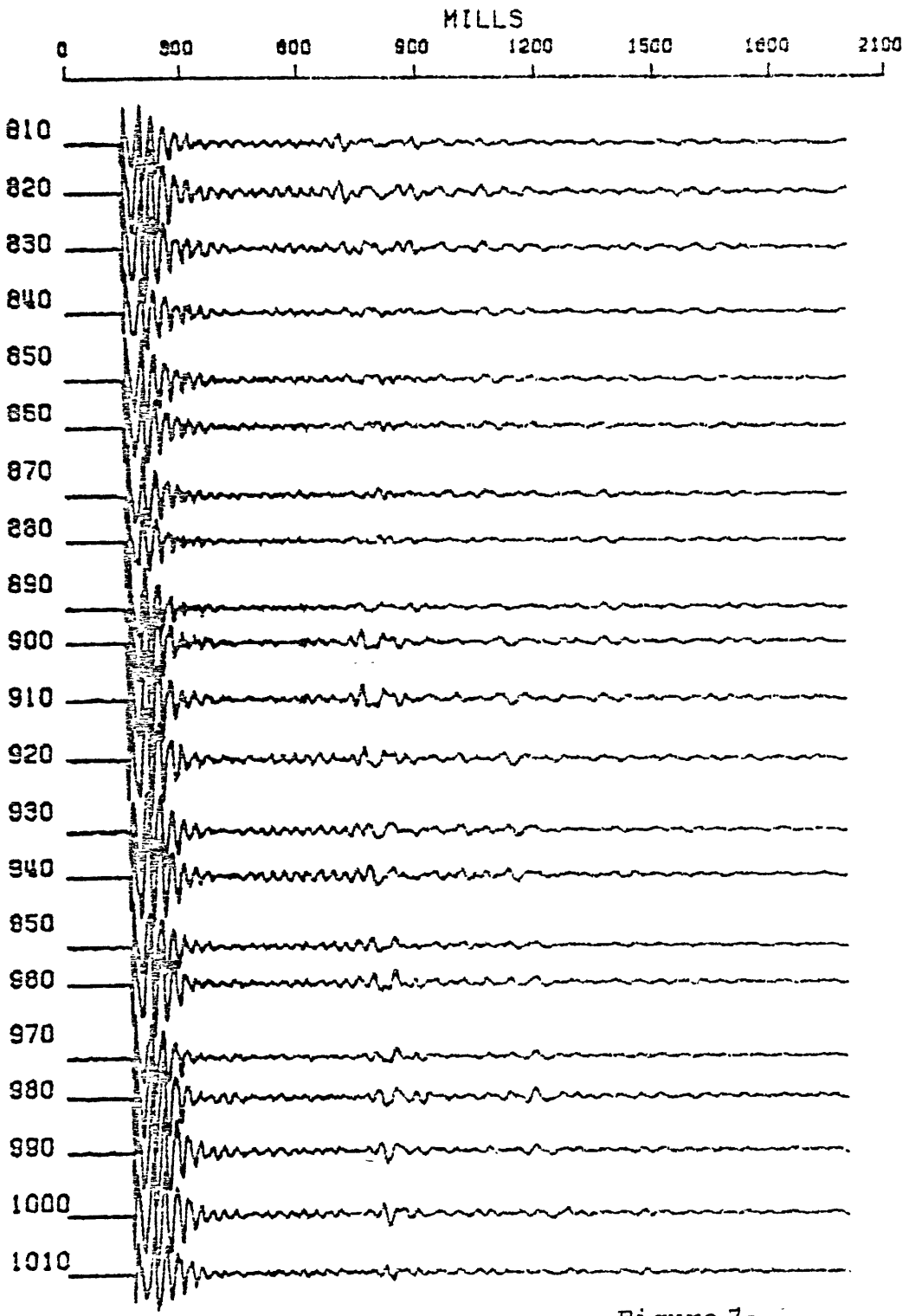
MILLS
0
300
600
900
1200
1500
1800
2100
810
820
830
840
850
860
870
880
890
900
910
920
930
940
950
960
970
980
990
1000
1010

Figure 7

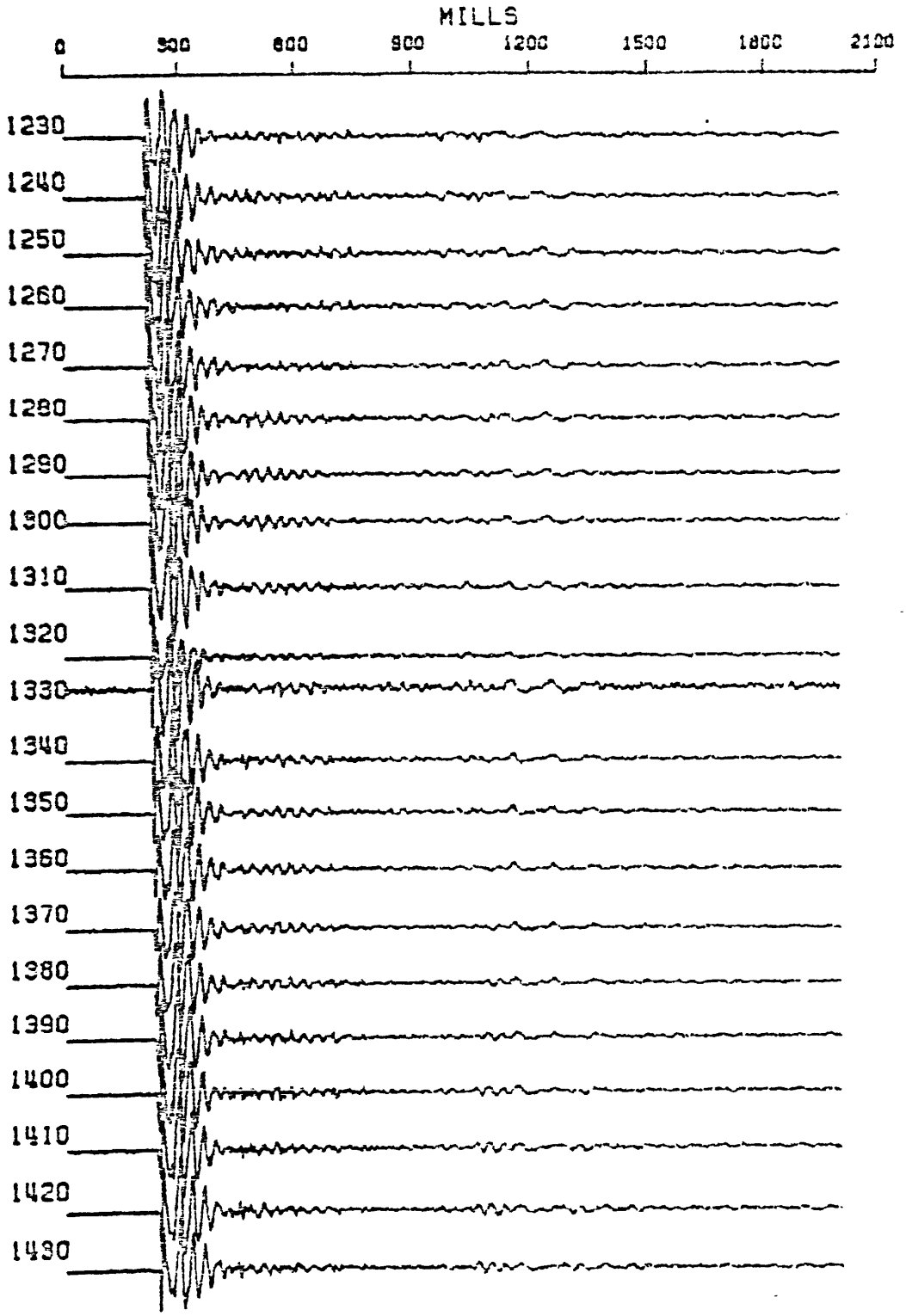
MILLS
0
500
800
900
1200
1500
1800
2100
1230
1240
1250
1260
1270
1280
1290
1300
1310
1320
1330
1340
1350
1360
1370
1380
1390
1400
1410
1420
1430

Figure 8

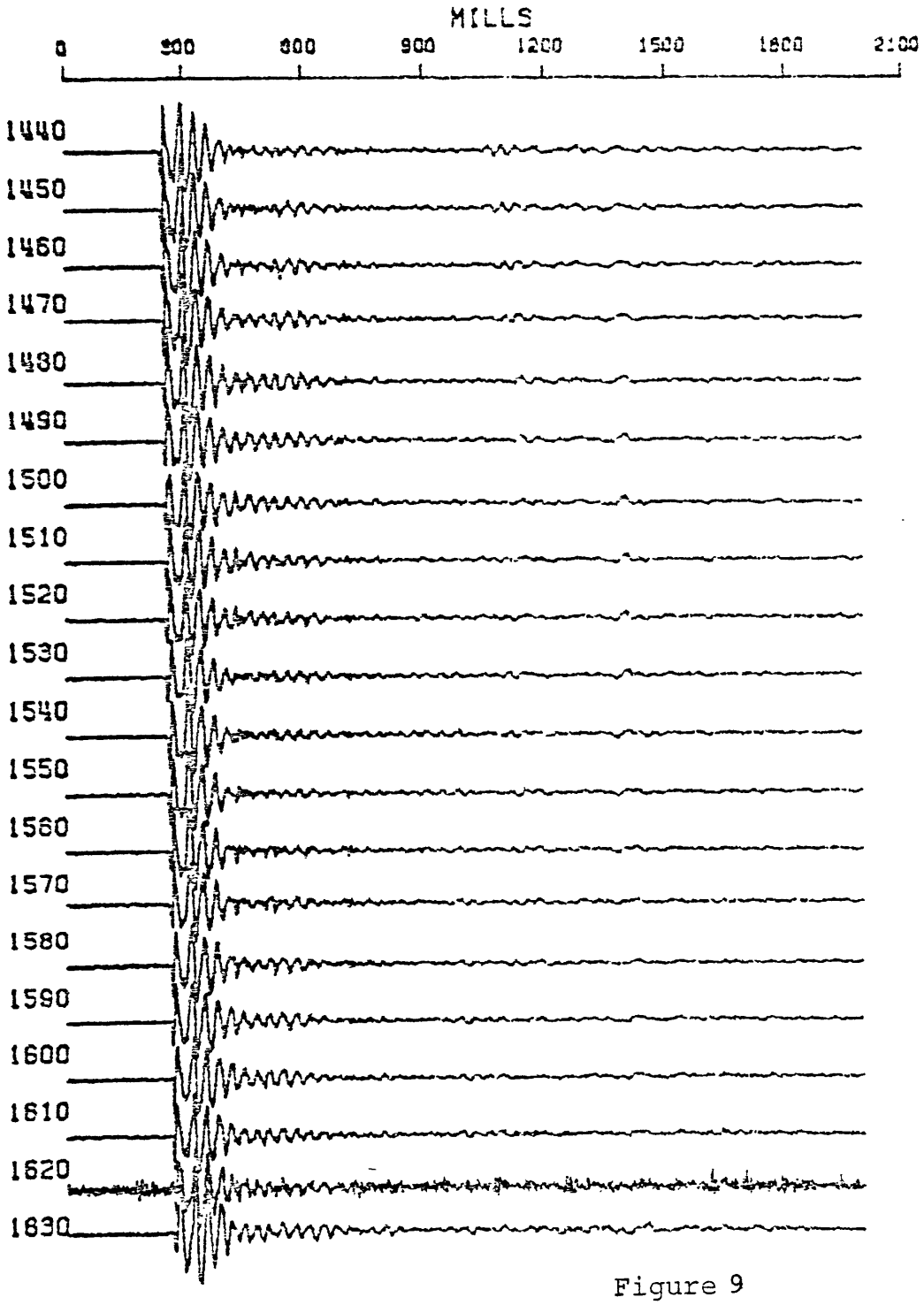
MILLS
0
300
600
900
1200
1500
1800
2100
1440
1450
1460
1470
1480
1490
1500
1510
1520
1530
1540
1550
1560
1570
1580
1590
1600
1610
1620
1630

Figure 9

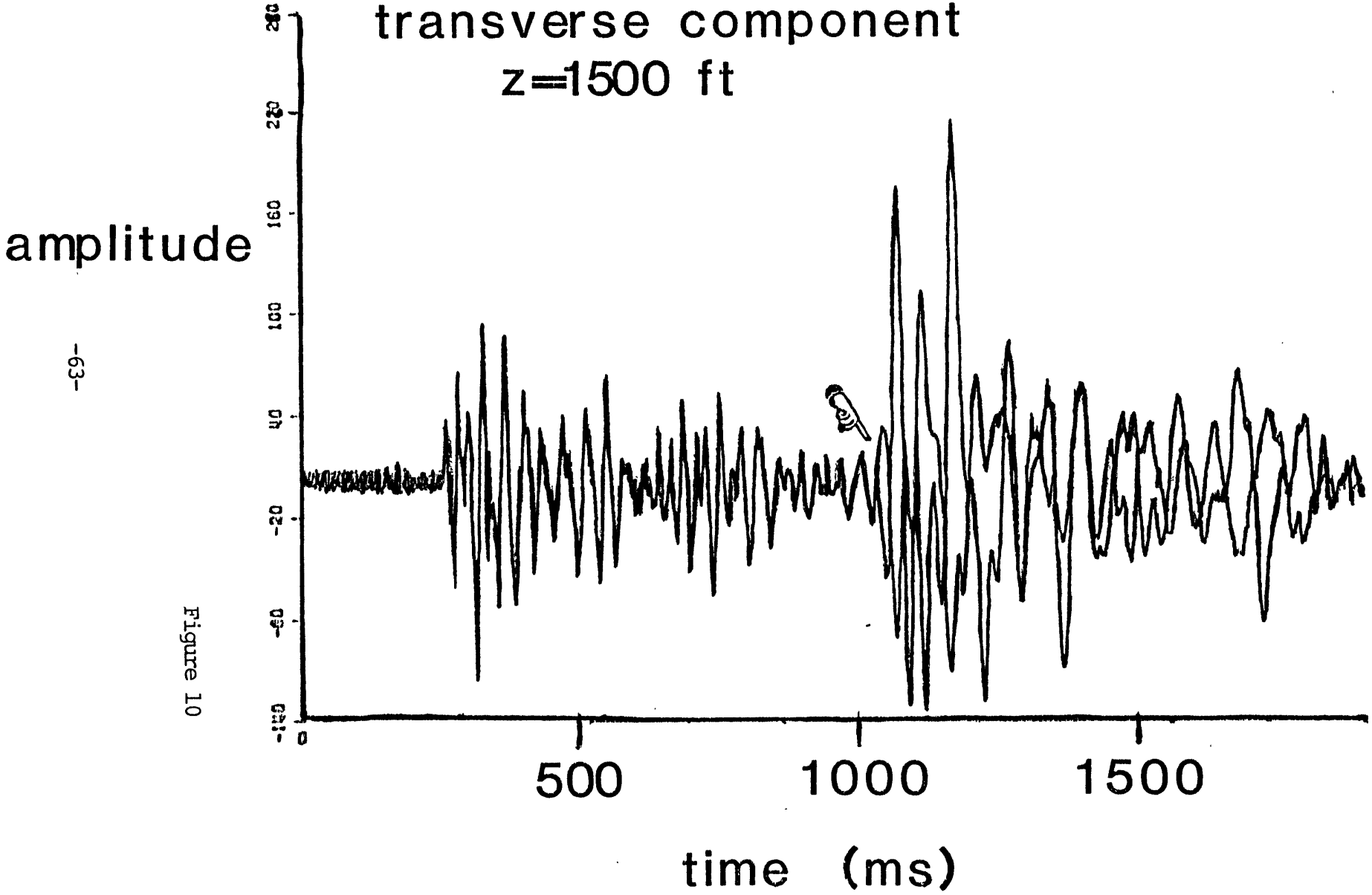
transverse component
z=1500 ft
amplitude
200
100
40
-20
-80
-120
0
500
1000
1500
time (ms)

Figure 10

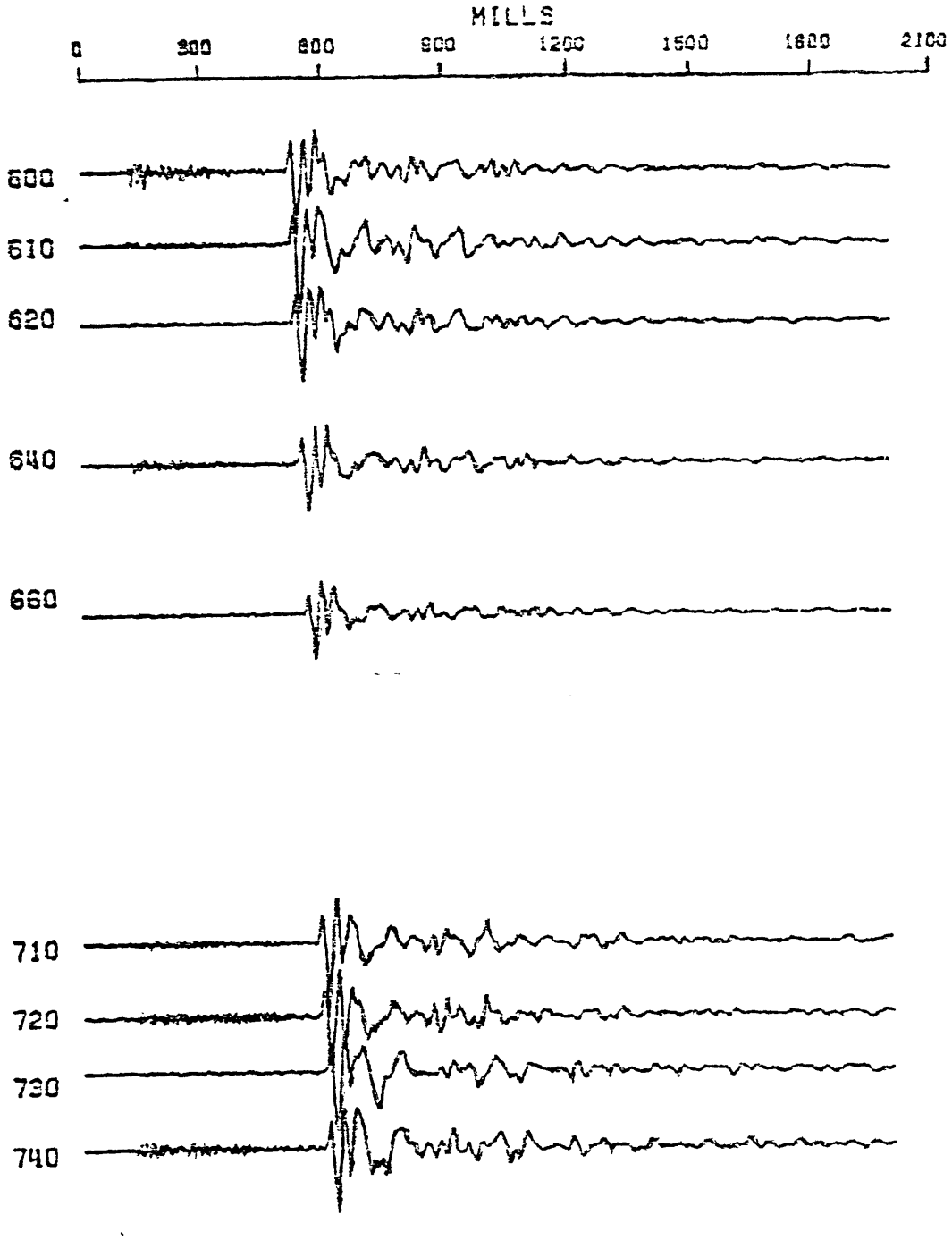
MILLS
0
300
600
900
1200
1500
1800
2100
600
610
620
640
660
710
720
730
740

Figure 11

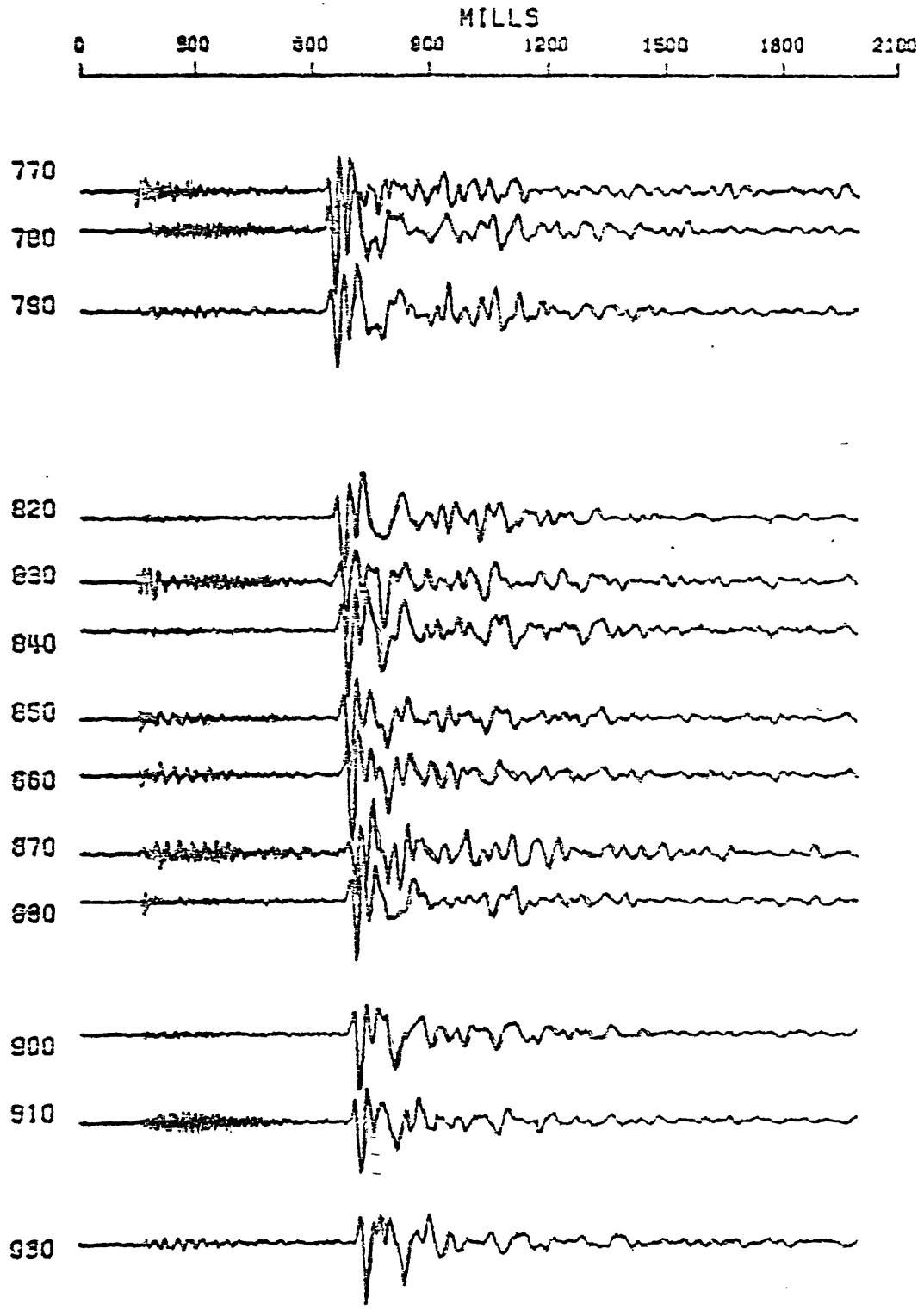
MILLS
0
900
600
900
1200
1500
1800
2100
770
780
790
820
830
840
850
860
870
880
900
910
930

Figure 12

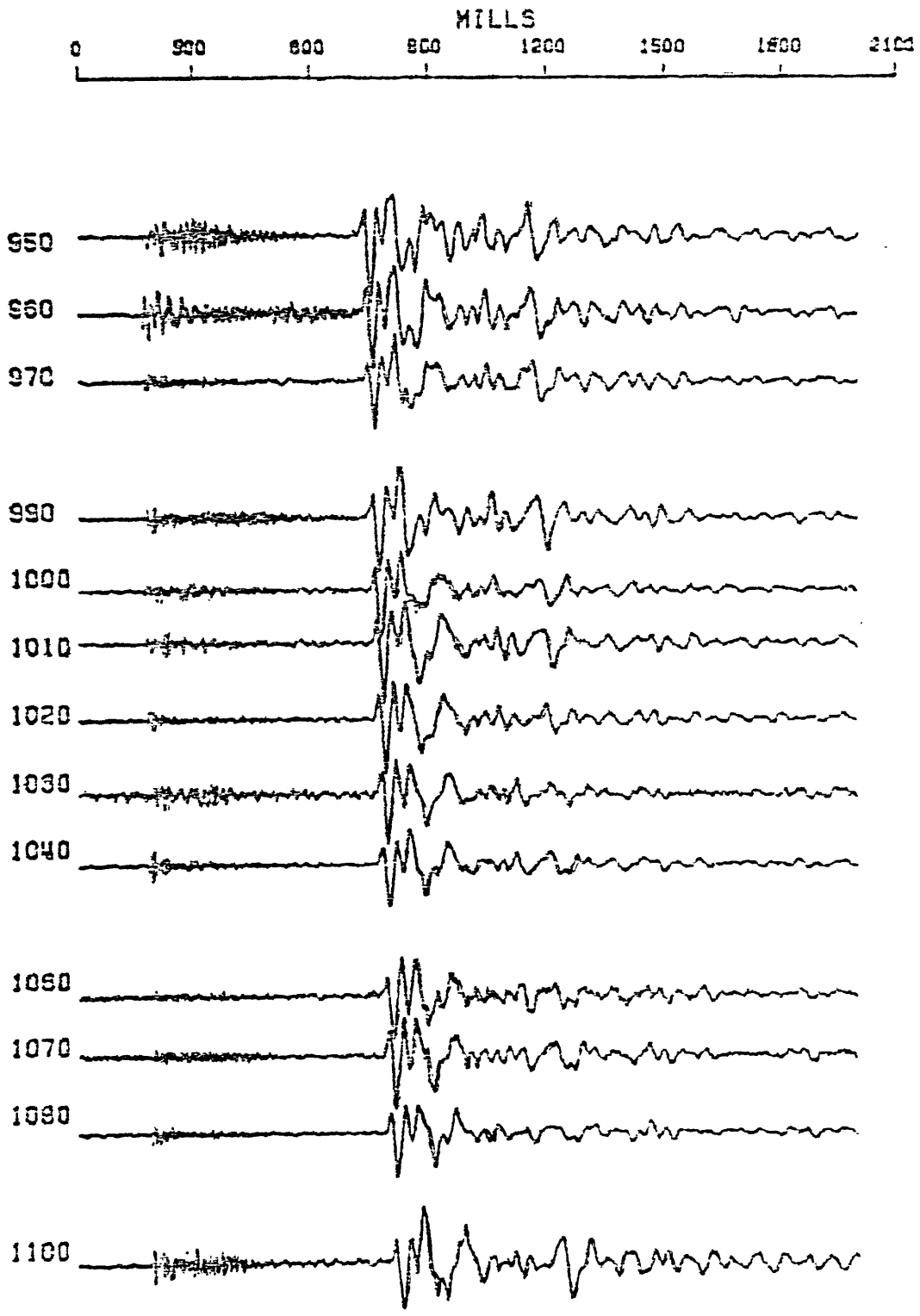
MILLS
0
900
800
1200
1500
950
960
970
990
1000
1010
1020
1030
1040
1060
1070
1080
1100

Figure 13

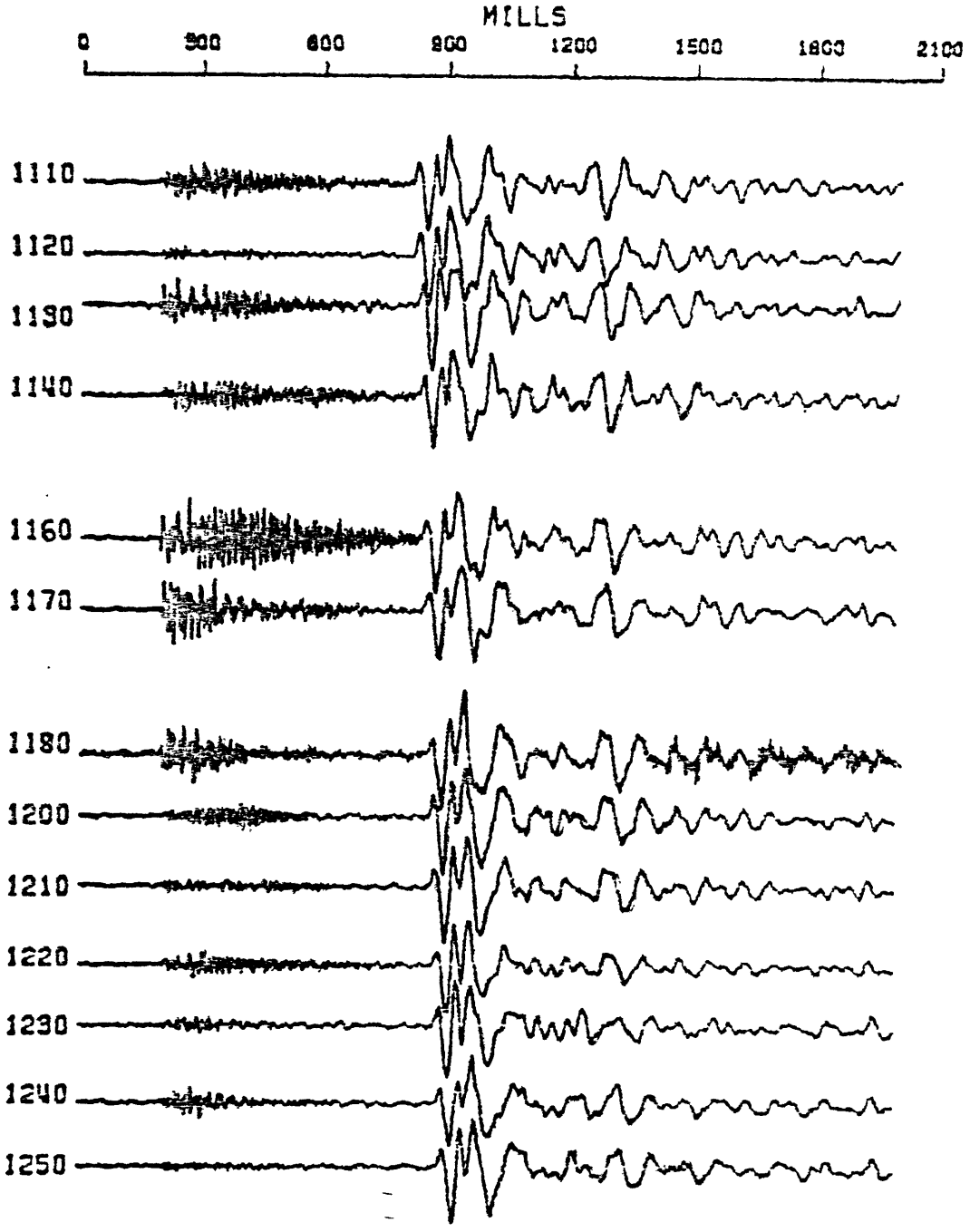
MILLS
0
300
600
900
1200
1500
1800
2100
1110
1120
1130
1140
1160
1170
1180
1200
1210
1220
1230
1240
1250

Figure 14

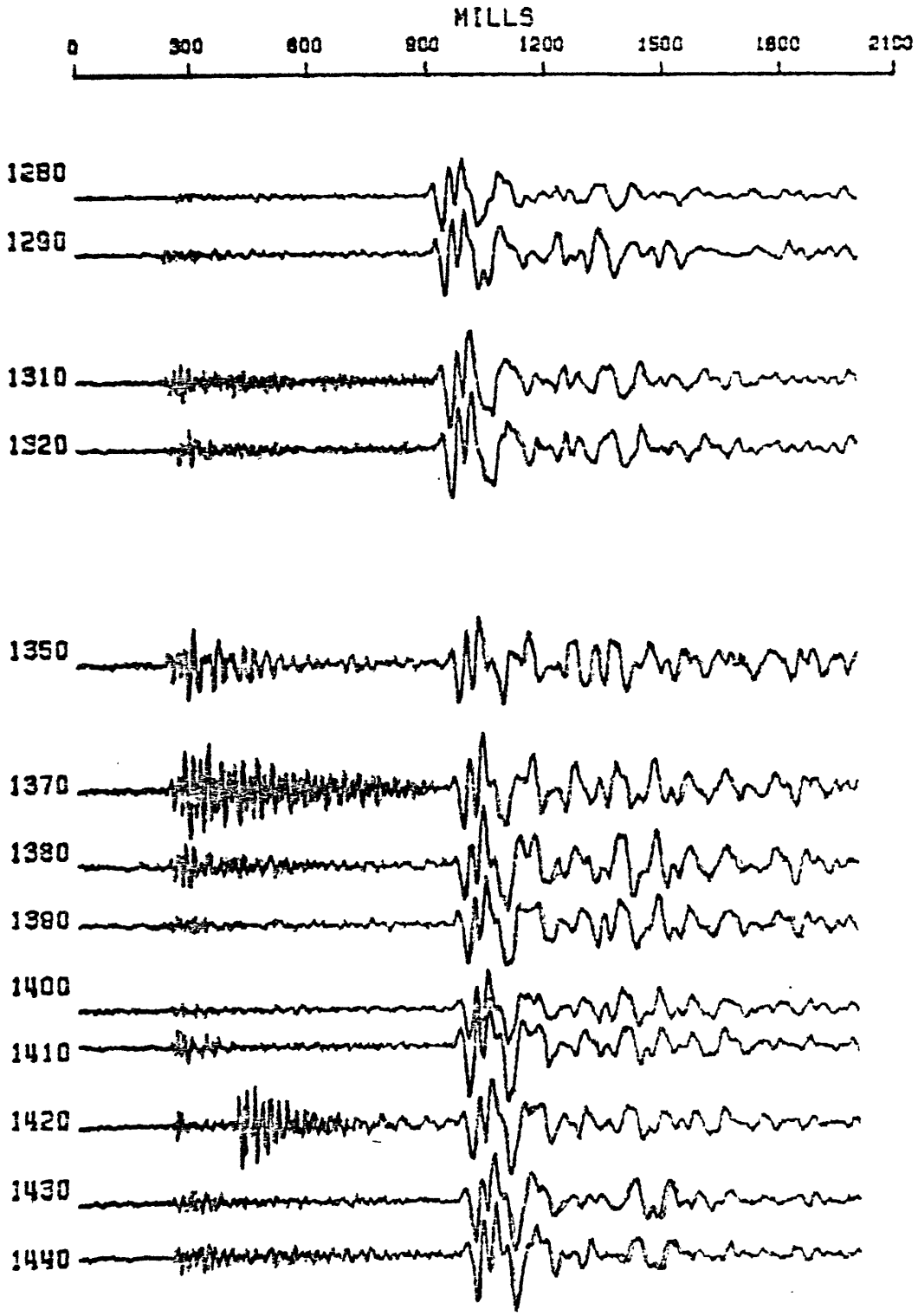
MILLS
0
300
600
900
1200
1500
1800
2100
1280
1290
1310
1320
1350
1370
1380
1390
1400
1410
1420
1430
1440

Figure 15

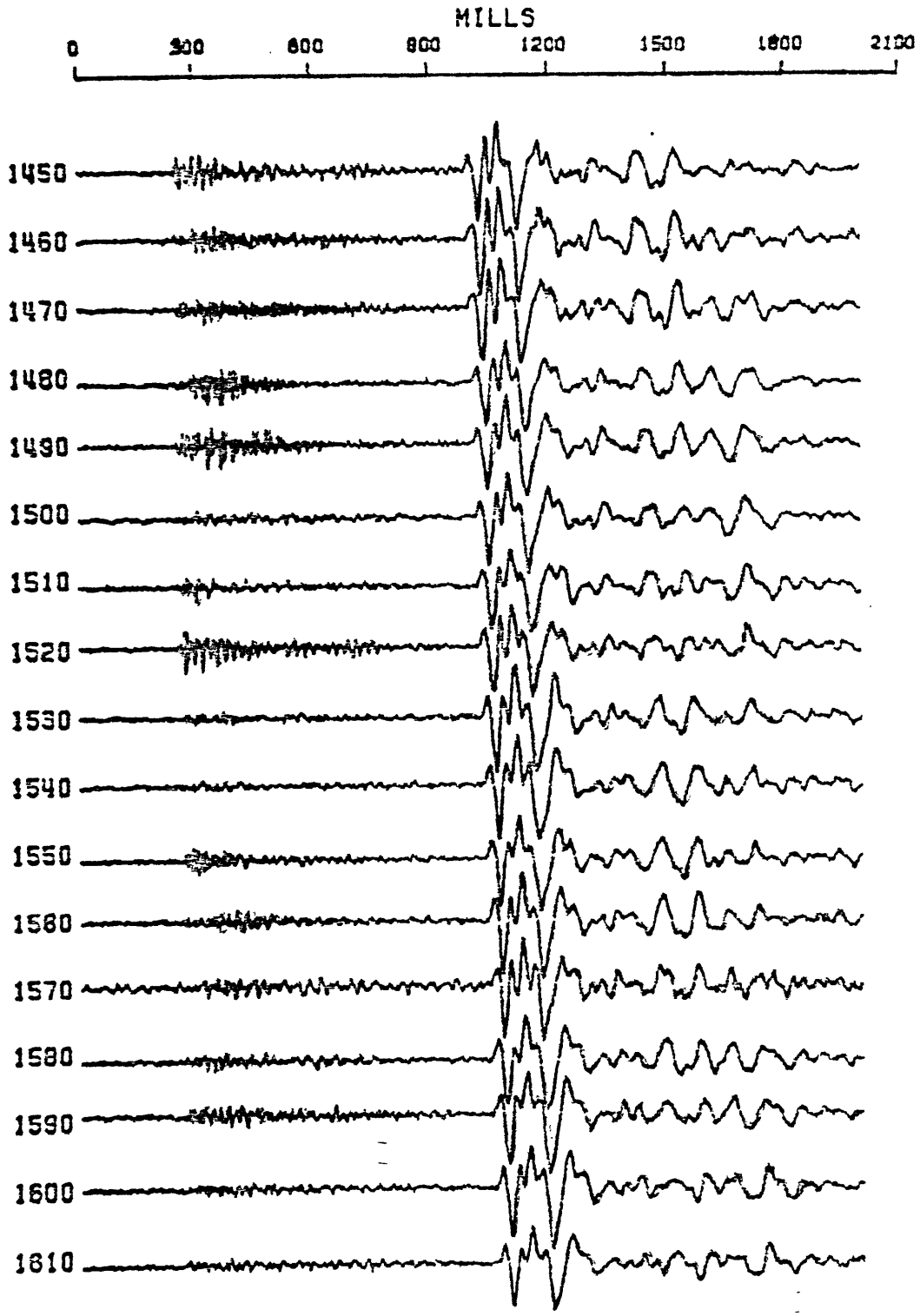
MILLS
0
300
600
900
1200
1500
1800
2100
1450
1460
1470
1480
1490
1500
1510
1520
1530
1540
1550
1560
1570
1580
1590
1600
1610

Figure 16

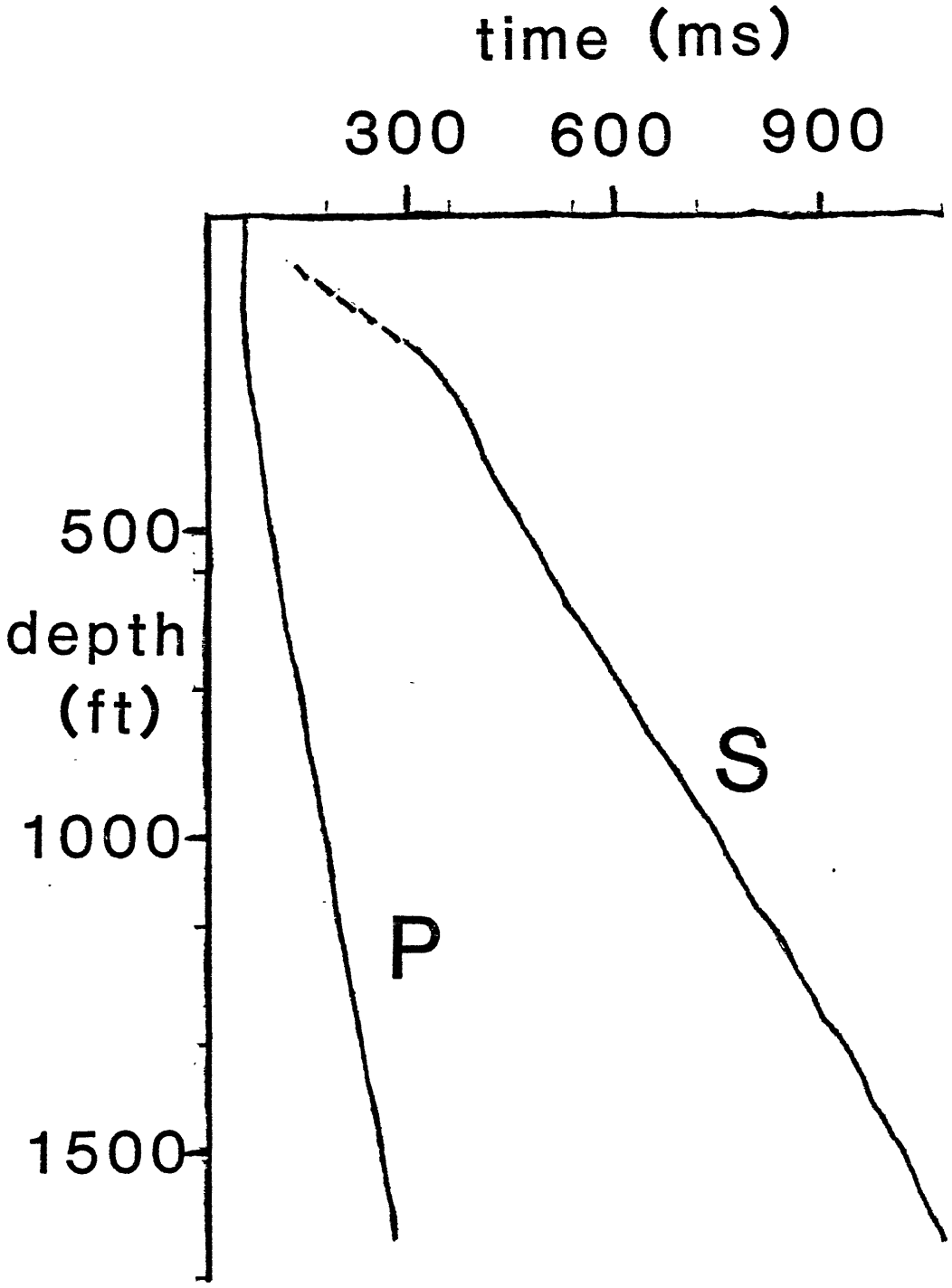

Figure 17

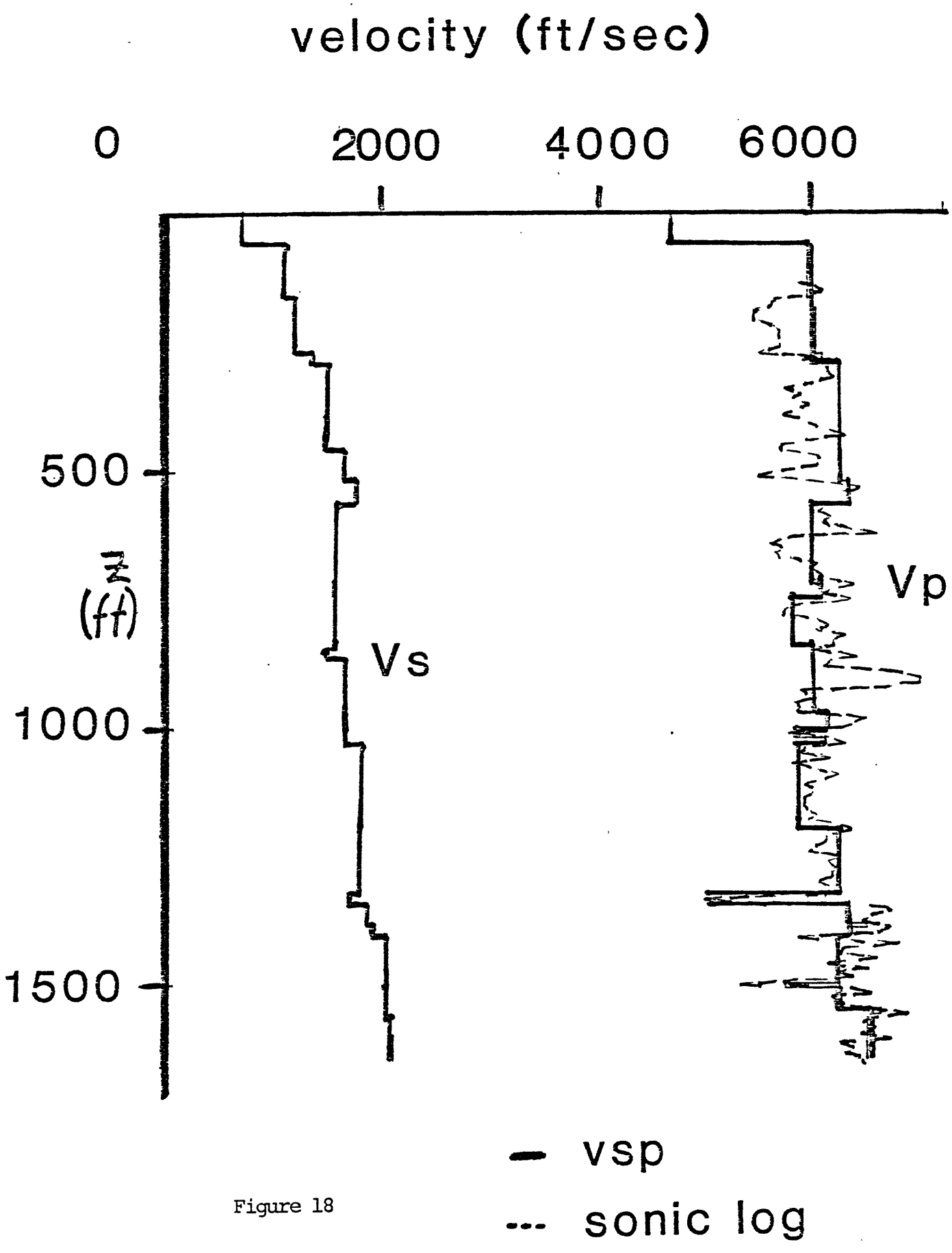
velocity (ft/sec)
0
2000
4000
6000
500
1000
1500
(ft)
Vs
Vp
vsp
sonic log

Figure 18

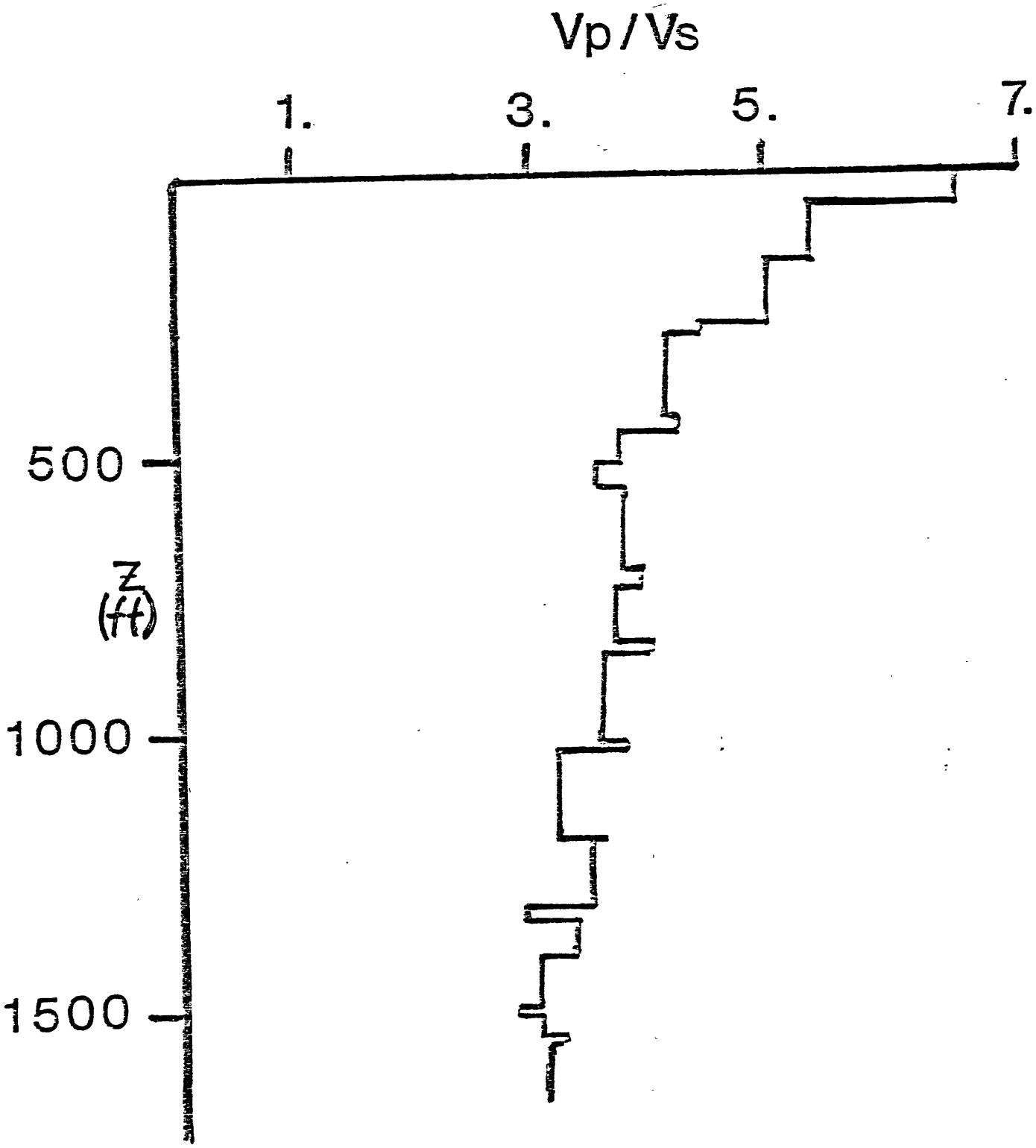

Figure 19

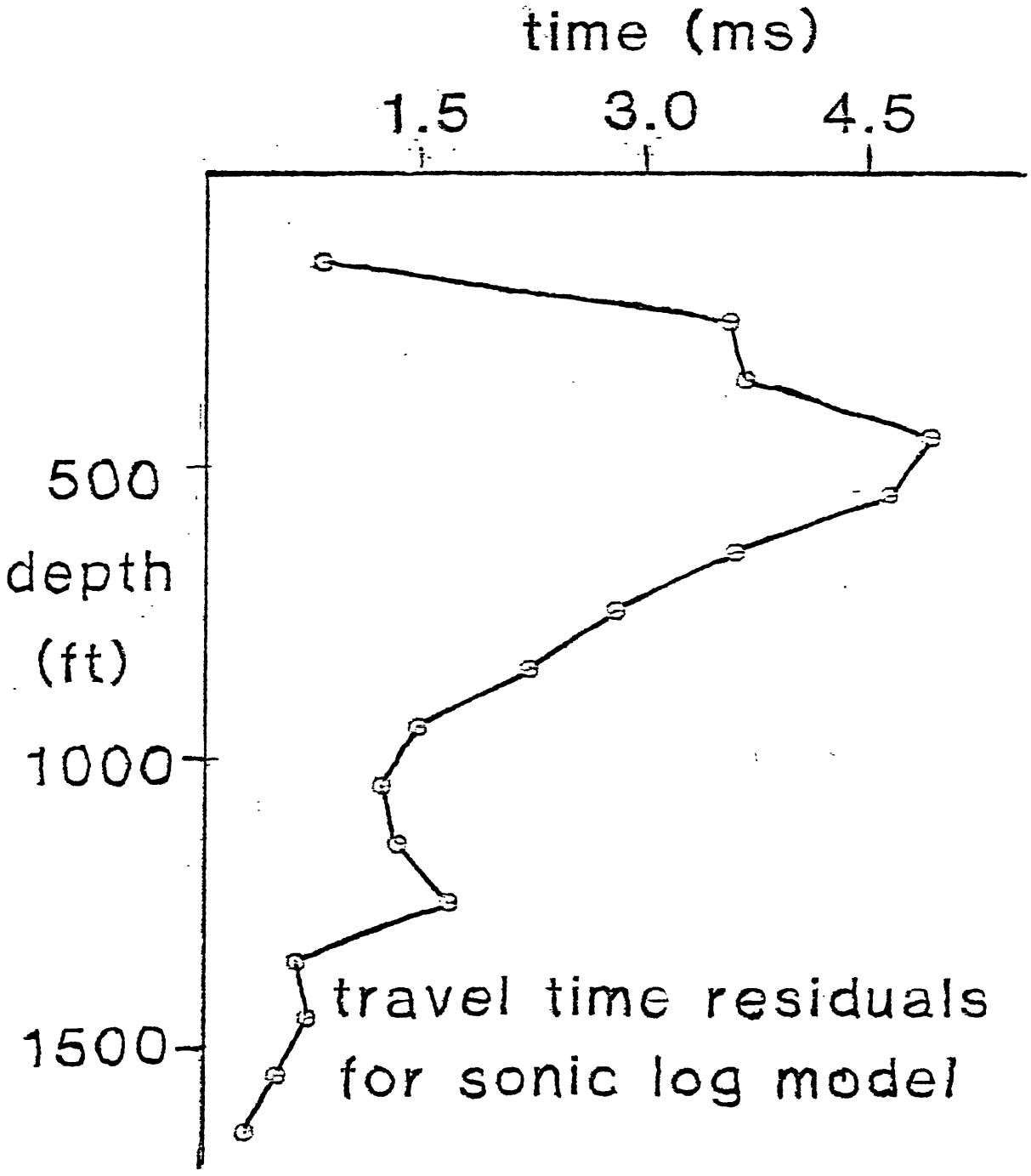
time (ms)
1.5
3.0
4.5
500
depth
(ft)
1000
1500
travel time residuals
for sonic log model

Figure 20

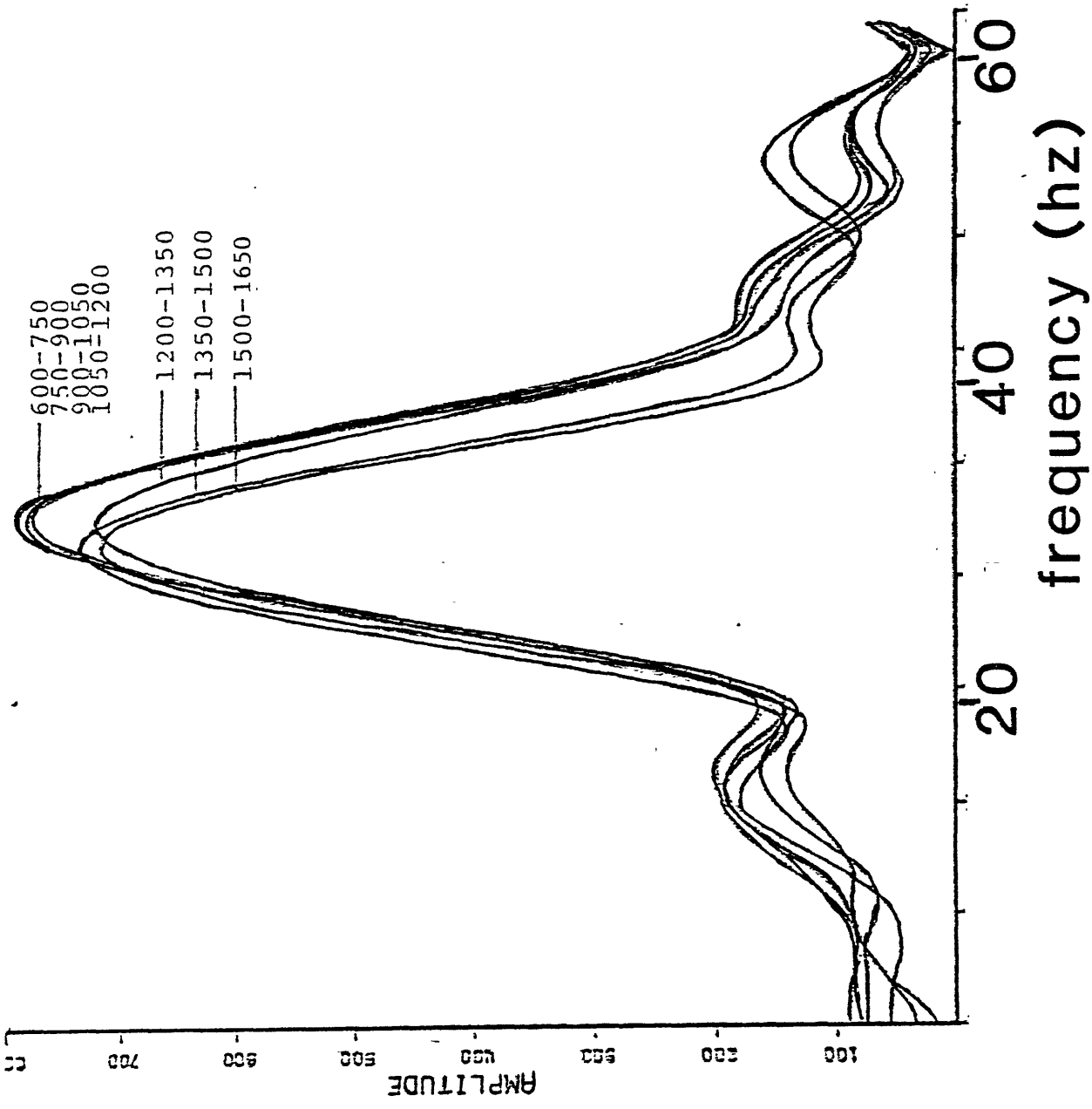
600-750
750-900
900-1050
1050-1200
1200-1350
1350-1500
1500-1650
frequency (hz)
20
40
60
AMPLITUDE

Figure 21

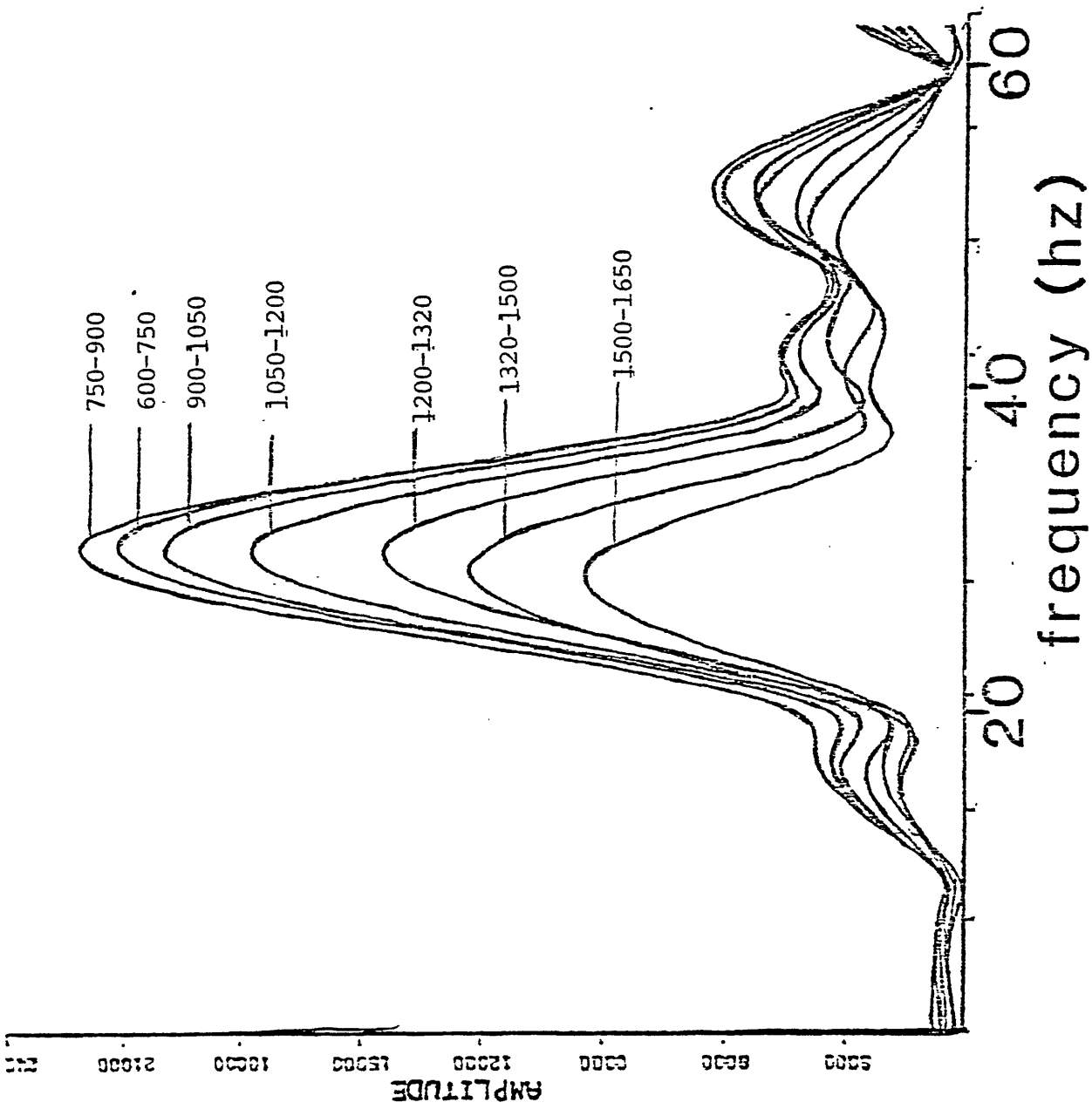
750-900
600-750
900-1050
1050-1200
1200-1320
1320-1500
1500-1650
20
40
60
frequency (hz)
AMPLITUDE

Figure 22

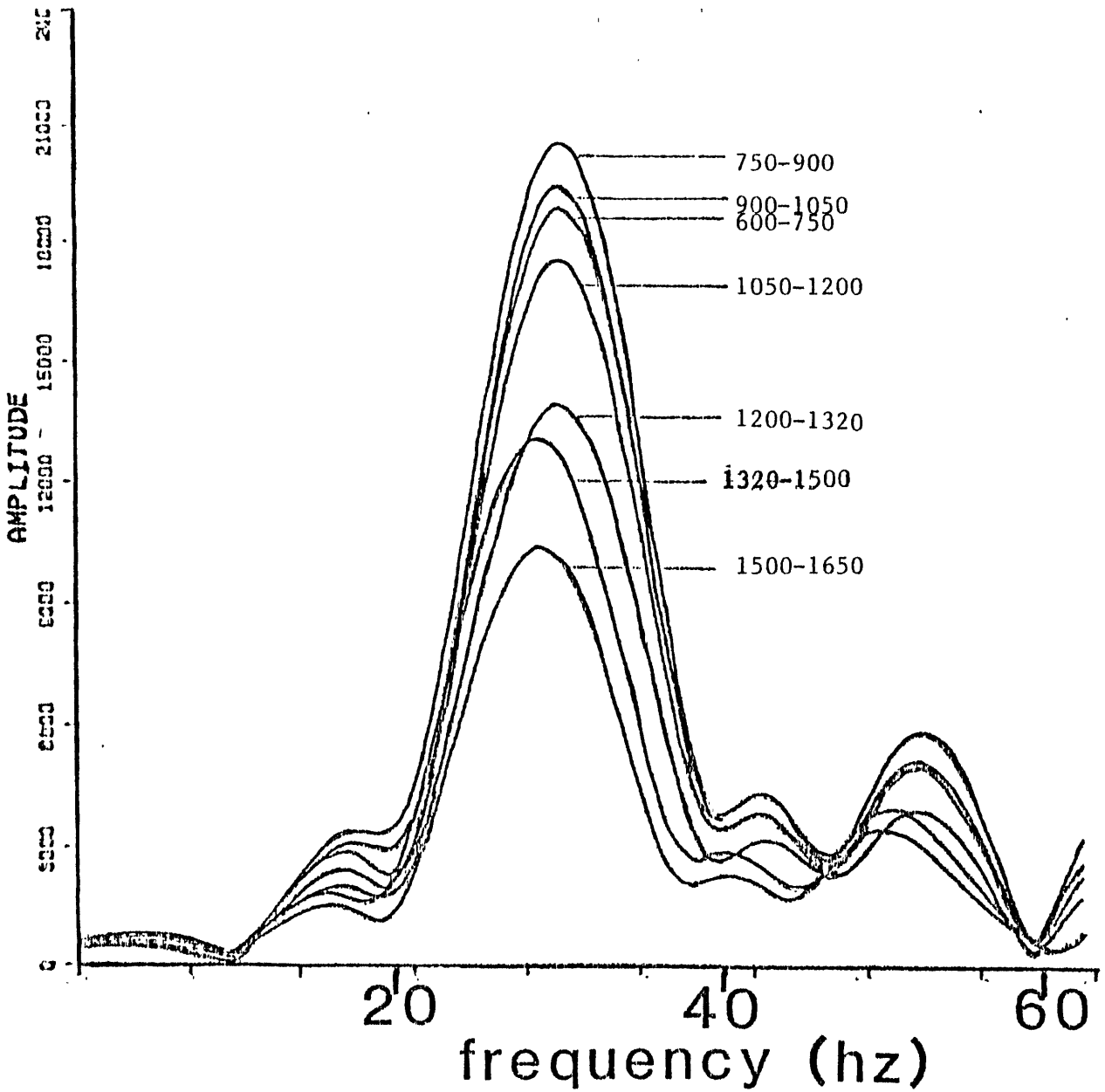
AMPLITUDE
750-900
900-1050
600-750
1050-1200
1200-1320
1320-1500
1500-1650
20
40
60
frequency (hz)

Figure 23

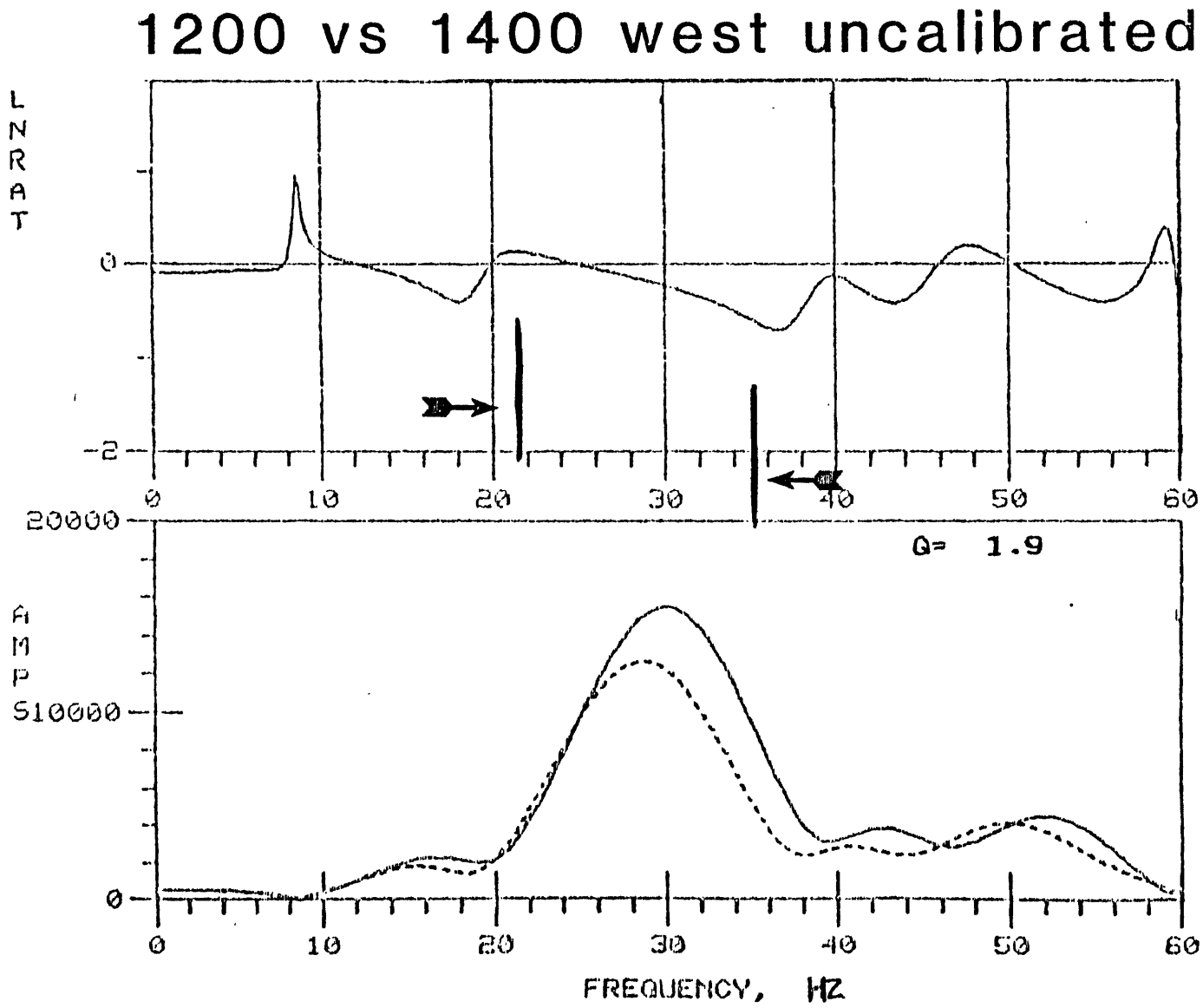
1200 vs 1400 west uncalibrated
LNRAT
0
-2
0
10
20
30
40
50
60
20000
Q= 1.9
AMP
S10000
0
0
10
20
30
40
50
60
FREQUENCY, HZ

Figure 24

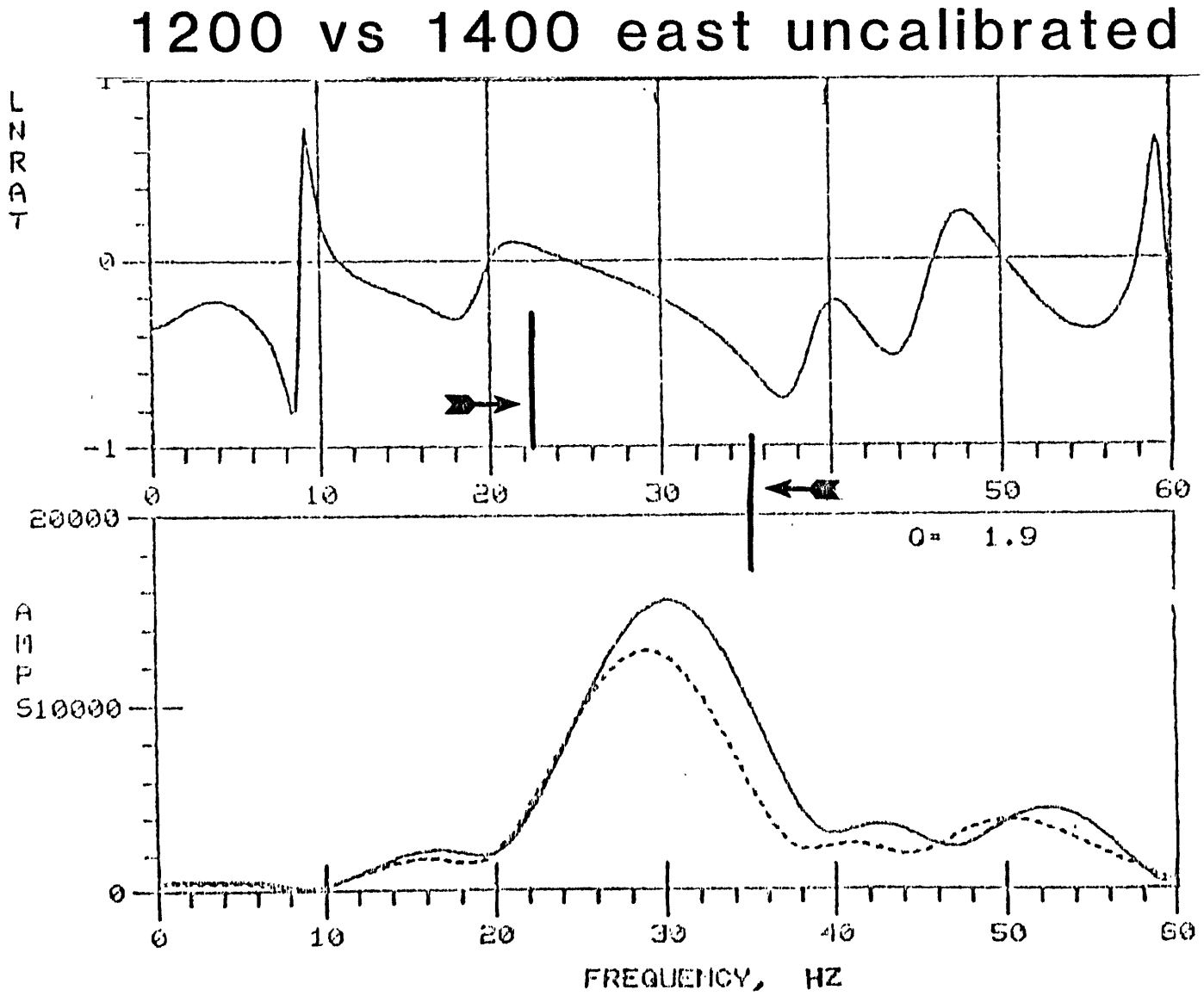
1200 vs 1400 east uncalibrated
LNRAT
1
0
-1
0
10
20
30
50
60
20000
Q= 1.9
AMP
S10000
0
0
10
20
30
40
50
60
FREQUENCY, HZ

Figure 25

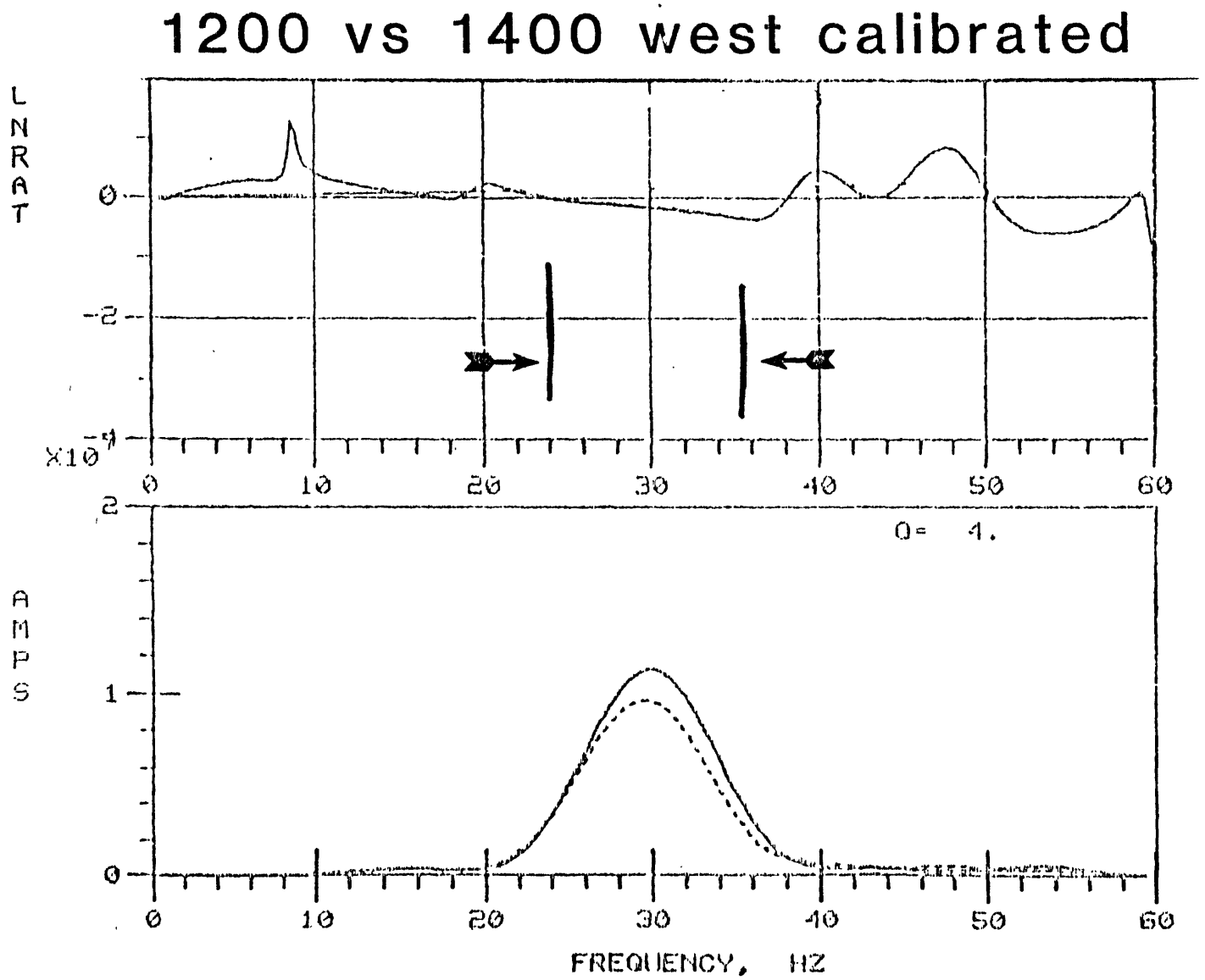
1200 vs 1400 west calibrated
LNRAT
0
-2
X10⁻⁴
0
10
20
30
40
50
60
2
1
0
AMPS
Q= 1.
0
10
20
30
40
50
60
FREQUENCY, HZ

Figure 26

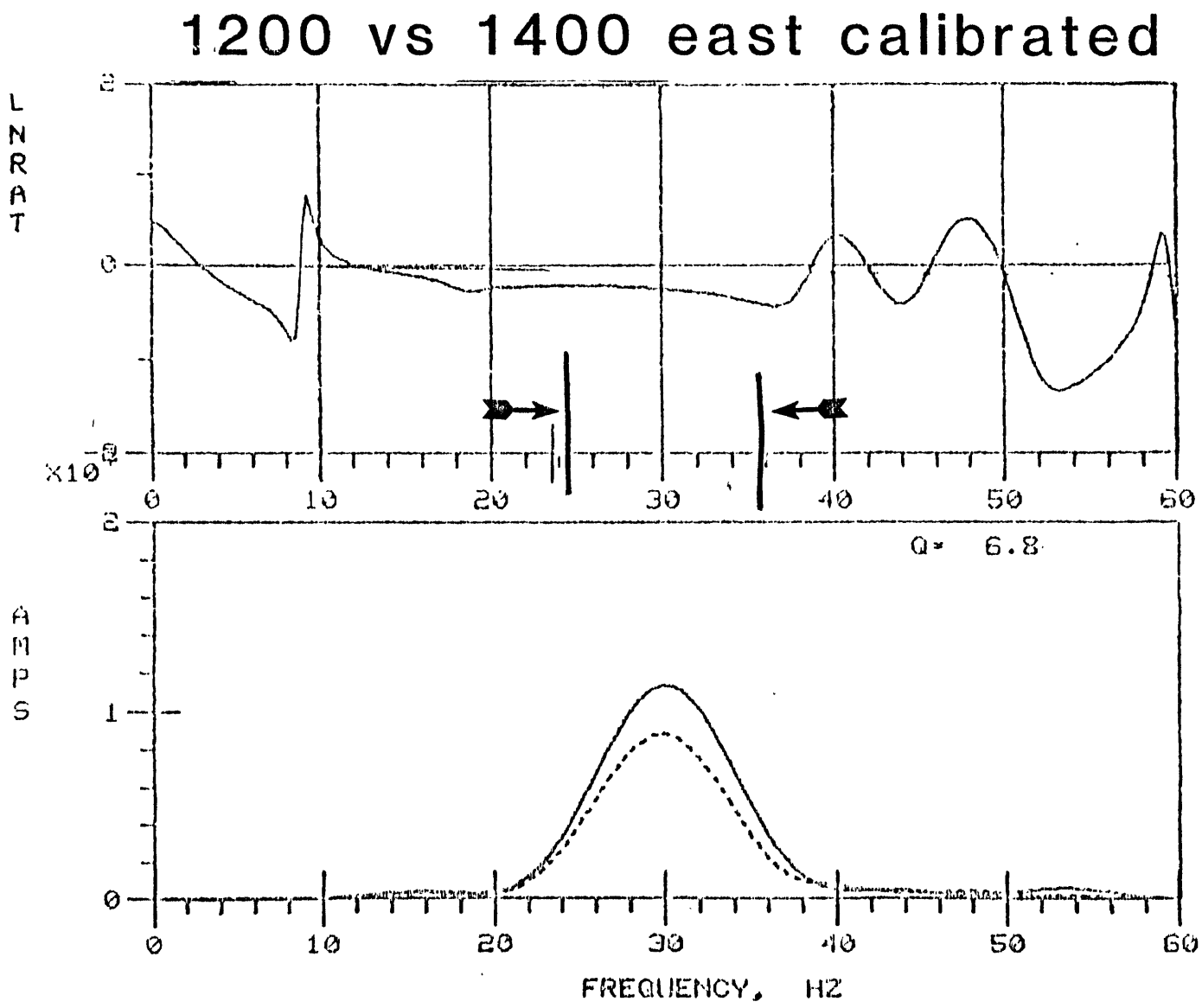
1200 vs 1400 east calibrated
LNRAT
X10
2
0
-2
0
10
20
30
40
50
60
Q= 6.8
AMPS
2
1
0
0
10
20
30
40
50
60
FREQUENCY, HZ

Figure 27

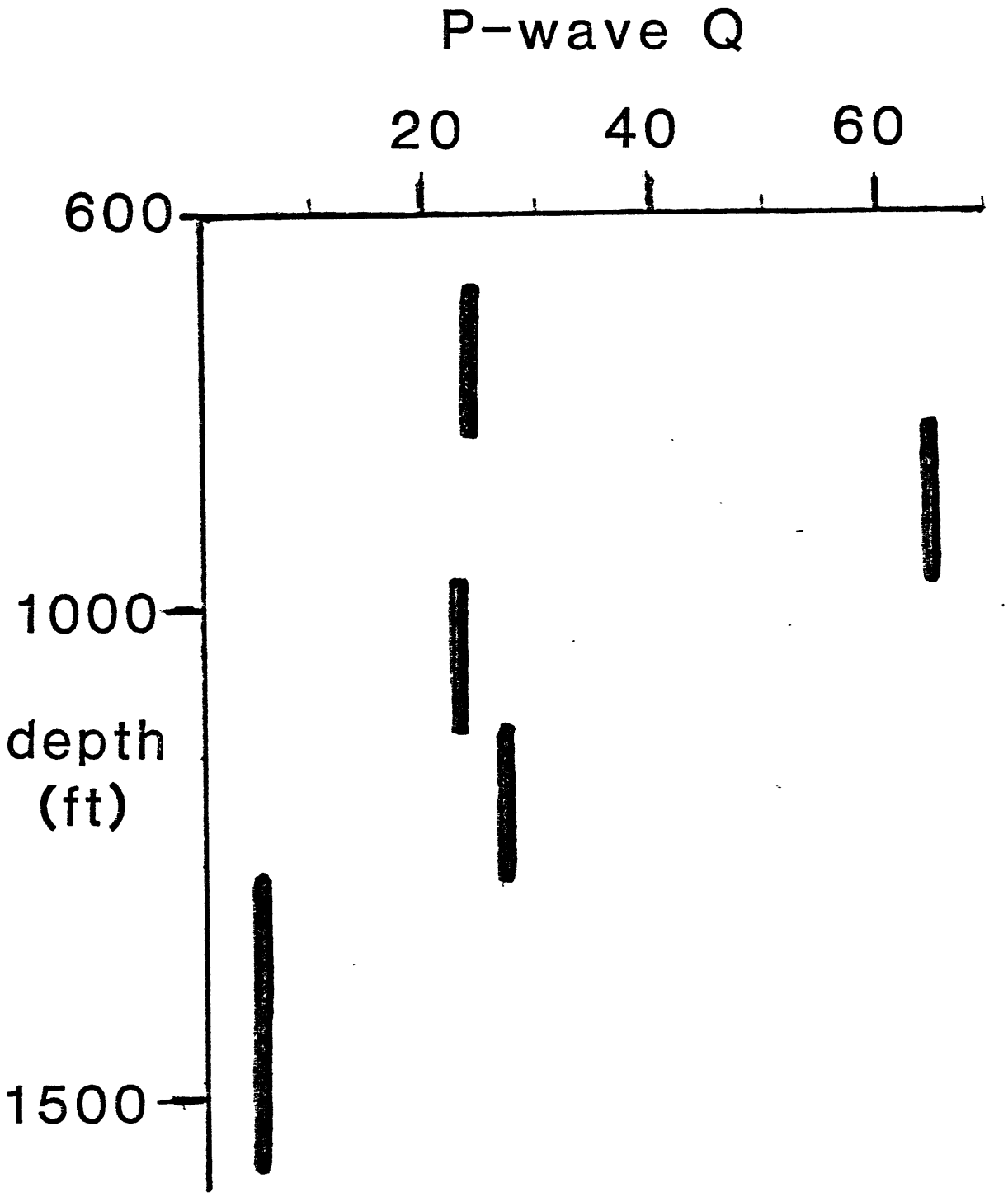

Figure 28

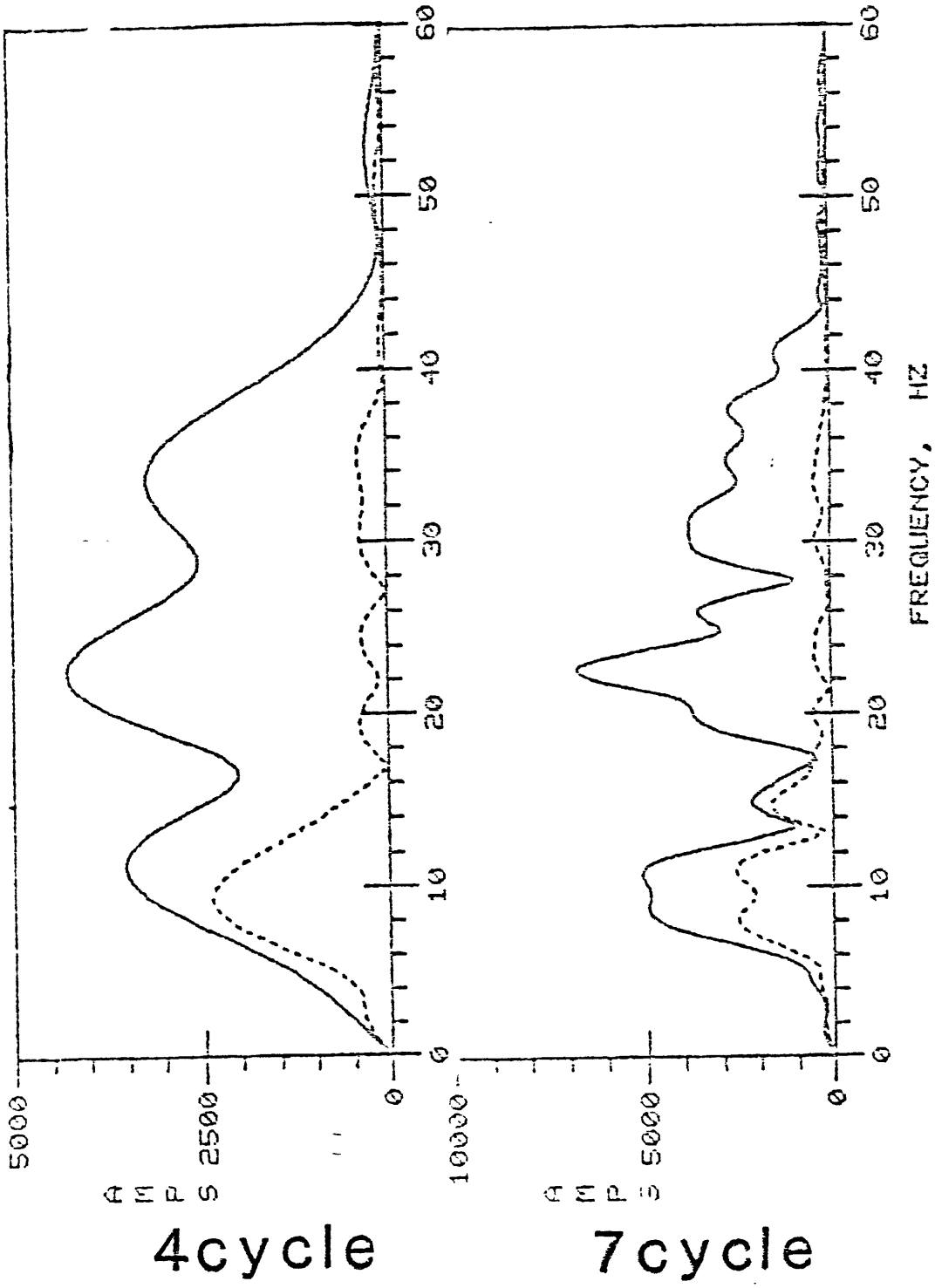
5000
2500
0
AMPS
4cycle
10000
5000
0
AMPS
7cycle
0
10
20
30
40
50
60
FREQUENCY, HZ

Figure 29

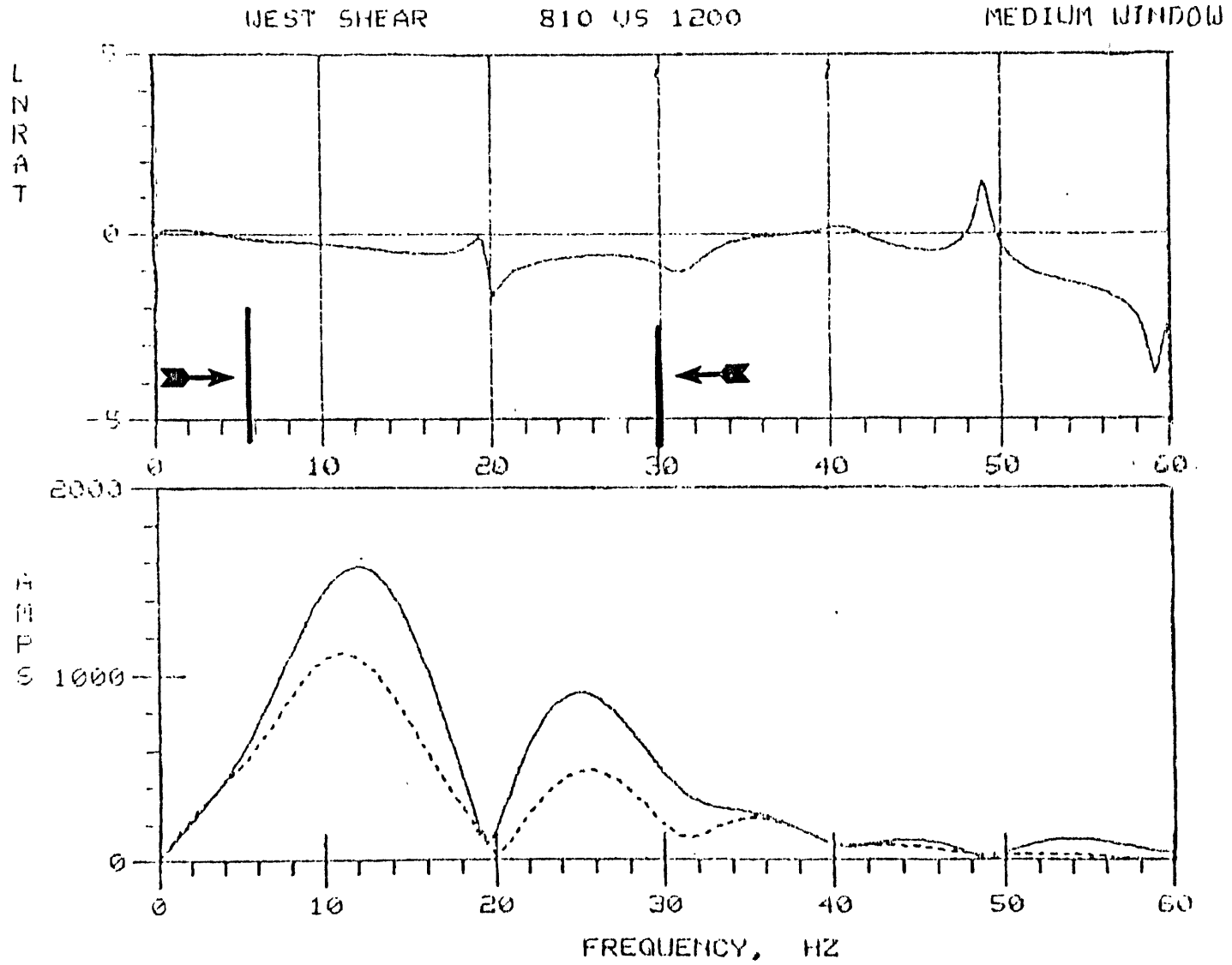
WEST SHEAR 810 US 1200 MEDIUM WINDOW
LNRAT
5
0
-5
0
10
20
30
40
50
60
2000
1000
0
FREQUENCY, HZ

Figure 30

Table 1

Velocity Relationships

Sediment Type	Vp	V_s	V_p/V_s
Sands	6090	1300	4.7
Silts	6075	1430	4.3
Shales	6050	1700	3.5
Top half	6010	1600	3.8
Lower half	6090	1820	3.4
All Types			
Top half	5930	1320	4.5
Bottom	6210	1750	3.6
Overall	6070	1540	4.0

Measured Body Wave Q For Several Rock Types

Rock	Q	Frequency, Hz	Method	Reference
Quincy Granite	125 166	(.14-4.5) x 10^3	long resonance tors. resonance	Birch and Bancroft (1938)
Solenhofen Limestone	112 188	(3-15) x 10^6	P wave pulses S wave pulses	Peselnick and Zietz (1959)
I-1 Limestone	165	(5-10) x 10^6	P wave pulses	Peselnick and Zietz (1959)
Hunton Limestone	65	(2.8-10.6) x 10^3	long. resonance	Born (1941)
Amherst Sandstone	52	(.930-12.8) x 10^3	long. resonance	Born (1941)
Berea Sandstone (brine saturated)	10	(.2-.8) x 10^6	P and S wave pulses	Toksöz et al. (1976)
Navajo Sandstone	21	50 - 120	flexural vibrations	Bruckshaw and Mahanta (1954)
Pierre Shale	32 10	50 - 450	P waves in situ S wave in situ	McDonel et al. (1958)

Table 2
From Johnson (1978)

Table 3

Depth	vs	Depth	Polarity	Q	Comments
675		825	West	16	Uncorrected
			East	32	"
825		975	West	41	"
			East	90	"
975		1125	West	11	"
			East	35	"
25		1275	West	11	"
			East	43	"
1275		1425	West	2	"
			East	2	"
1425		1575	West	5	"
			East	-15	"

Table 4

Depth	vs	Depth	Polarity	Q	Comments
675		825	West	10	Corrected
			East	10	"
825		975	West	87	"
			East	-76	"
975		1125	West	-32	"
			East	-25	"
1125		1275	West	35	"
			East	83	"
1275		1425	West	5	"
			East	5	"
1425		1575	West	15	"
			East	32	"

Table 5

Depth	vs	Depth	Polarity	Q	Comments
1220-1310		1320-1510	West	2	Uncorrected
			East	2	"
			West	4	Corrected
			East	7	"

Table 6

Shear Wave Q Values

Depth1	vs	Depth2	Q	Polarity	Spectral Window
600-990		970-1,320	13	East	5-13 hz
			25	East	5-39 hz
			12	West	5-37 hz
810-1,200		1,200-1,600	41	East	5-14 hz
			10	East	5-33 hz
			50	West	5-15 hz
970-1,320		1,320-1,650	50	East	5-14 hz
			10	East	5-33 hz
			10	West	5-14 hz